

# Supporting information

## GSH resistant, Luminescent 2-(pyren-1-yl)-1H-imidazo[4,5-f][1,10]phenanthroline-based Ru(II)/Ir(III)/Re(I) Complexes for Phototoxicity in Triple Negative Breast Cancer Cell

Rishav Das, Priyankar Paira\*

### Index

### PageNo.

Fig. S1: UV- VIS spectra of RuL IrL ReL complexes in 10% DMSO	2
Fig. S2: Fluorescence spectra of complexes in 10% DMSO while excited in $\pi$ - $\pi^*$ region	2
Fig. S3: Fluorescence spectra of complexes in 10% DMSO while excited in MLCT region	3
Fig. S4: Stability study of complexes in GSH medium	3-4
Fig. S5: Stability study of complexes in 10% DMSO	5-6
Fig. S6: Stability study of complexes in presence of cystine	6-7
Fig. S7: $^1\text{H}$ NMR spectroscopic study on the stability of complexes in presence of cystine	8-9
Fig. S8: Interaction of complexes (RuL, IrL, & ReL) with base pairs (adenine and guanine)	9-12
Fig. S9: DNA binding plot of (a) RuL (b) IrL and (c) ReL complexes	12-13
Fig. S10: $\{[\text{DNA}]/e_0 - e_f\} \times 10^{-12}$ vs. $[\text{DNA}]$ linear plot of complexes	14-15
Fig. S11: Plot of fluorescence quenching EtBr-DNA with increasing complexes	15-16
Fig. S12: Stern-Volmer plot $I_0/I$ vs. concentration of complexes	17-18
Fig. S13: Relative viscosity plot of ct-DNA with complexes with respect to EtBr	18
Fig. S14: Interaction of complexes with BSA	19-20
Fig. S15: Stern-Volmer plot $I_0/I$ vs. concentration of complexes. Scatchard plot of $\log [I_0 - I/I]$ vs. $\log [\text{complex}]$ for BSA in presence of complexes	20-23
Fig. S16: Change in absorbance of DPBF with RB (Rose Bengal), RuL, IrL & ReL in the absence and presence of light	24-27
Fig. S17: Plot of relative change of absorbance ( $A/A_0$ ) vs. time (sec) of RB (Rose Bengal), RuL, IrL & ReL	28
26-27	
Characterization	29-38
Experimental Procedure	38-41
References	41-42

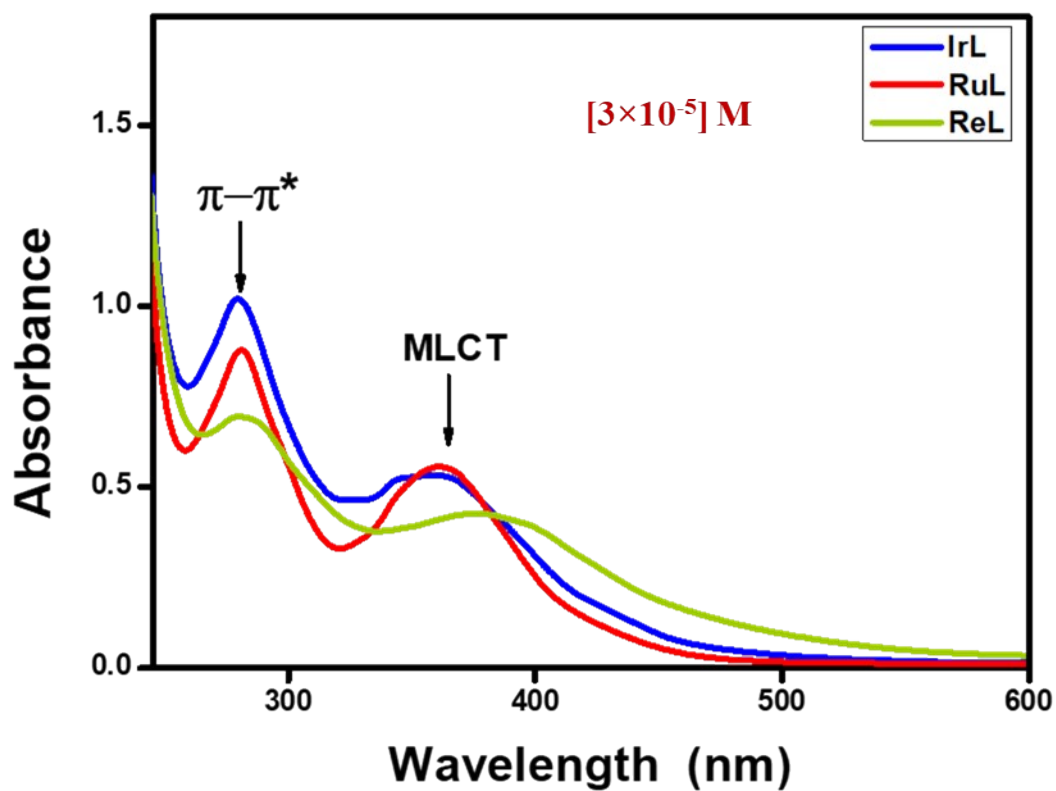


Fig. S1: UV- Vis spectra of RuL, IrL, and ReL complexes in 10% DMSO

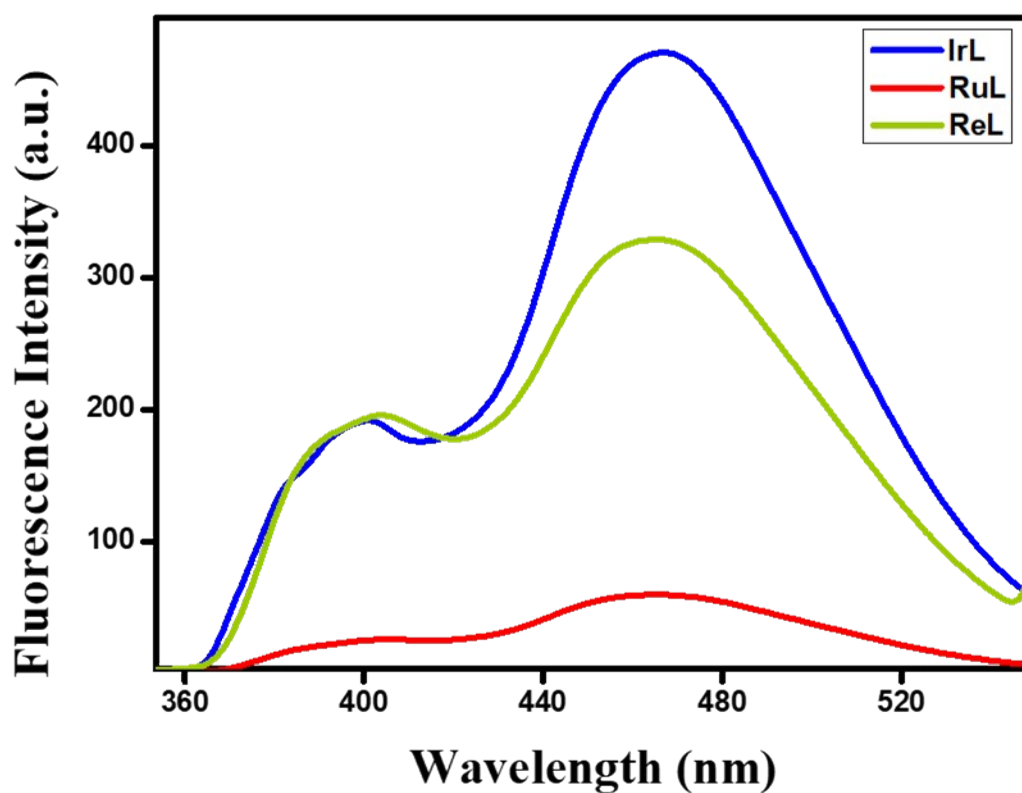


Fig. S2: Fluorescence spectra of RuL, IrL, and ReL complexes in 10% DMSO while excited in  $\pi-\pi^*$  region

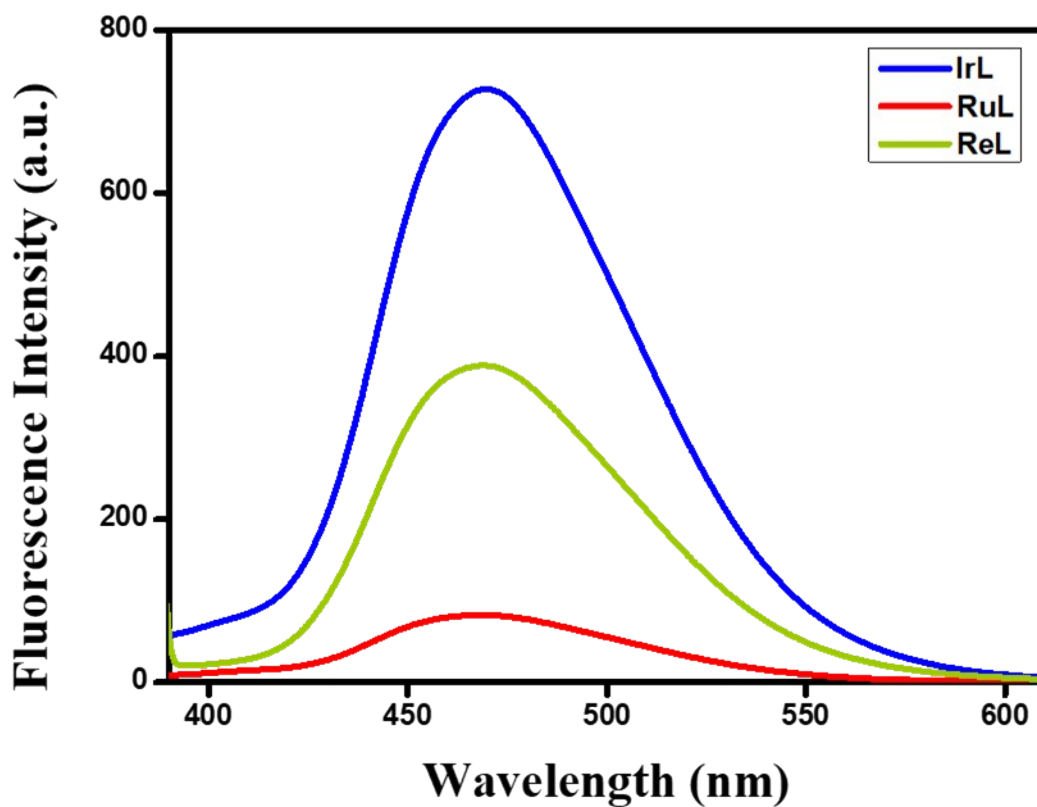
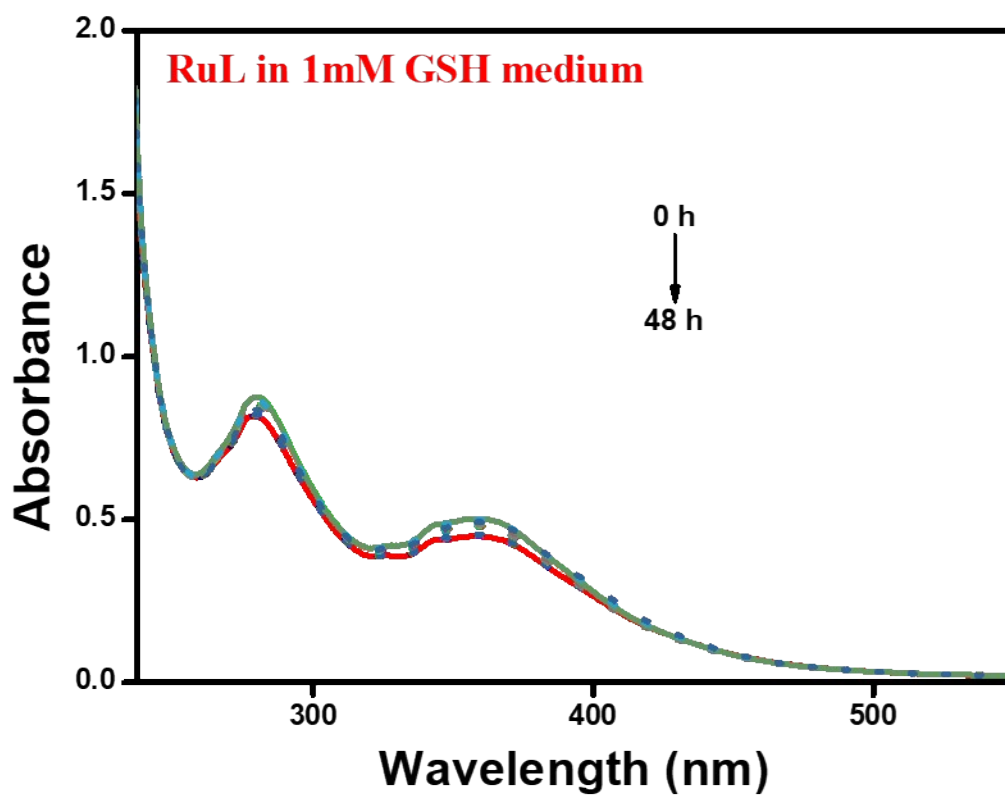
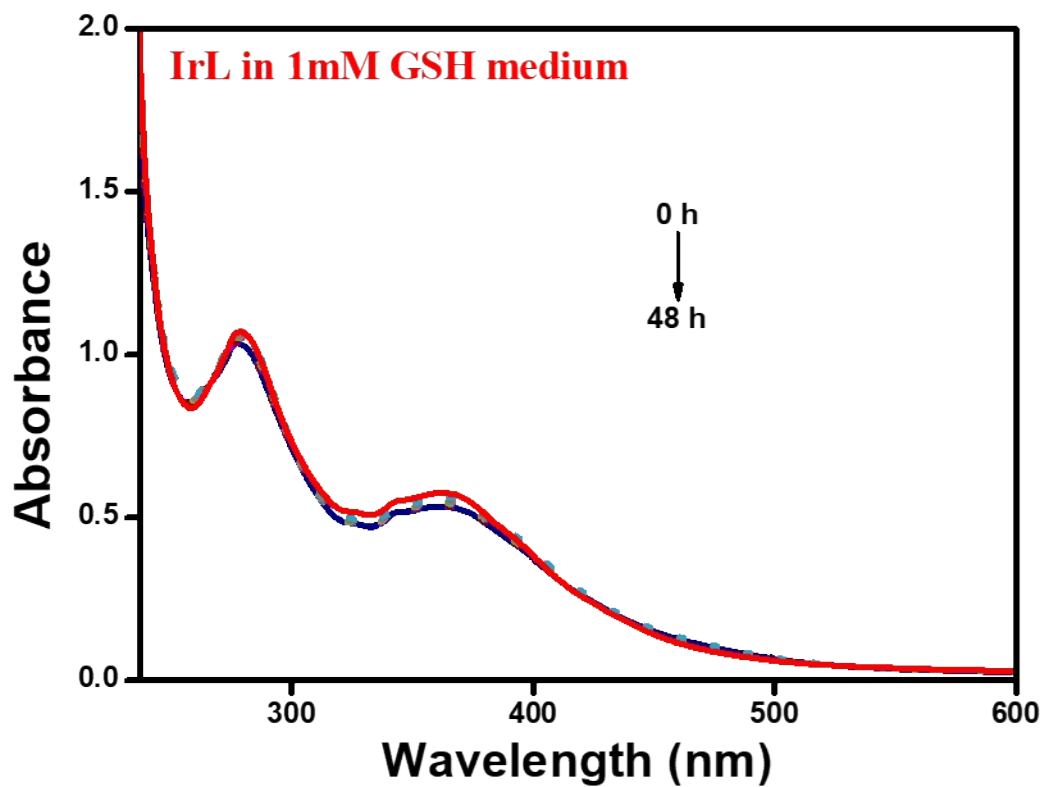


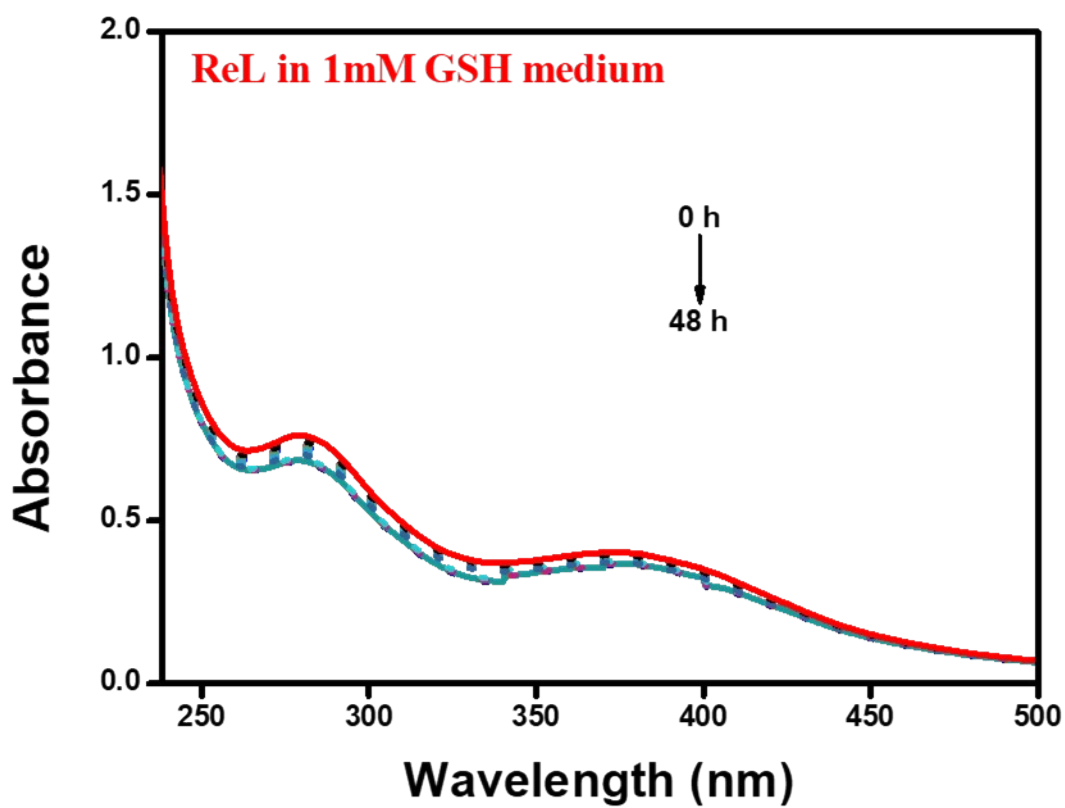
Fig. S3: Fluorescence spectra of RuL, IrL, ReL complexes in 10% DMSO while excited in MLCT region



(a)

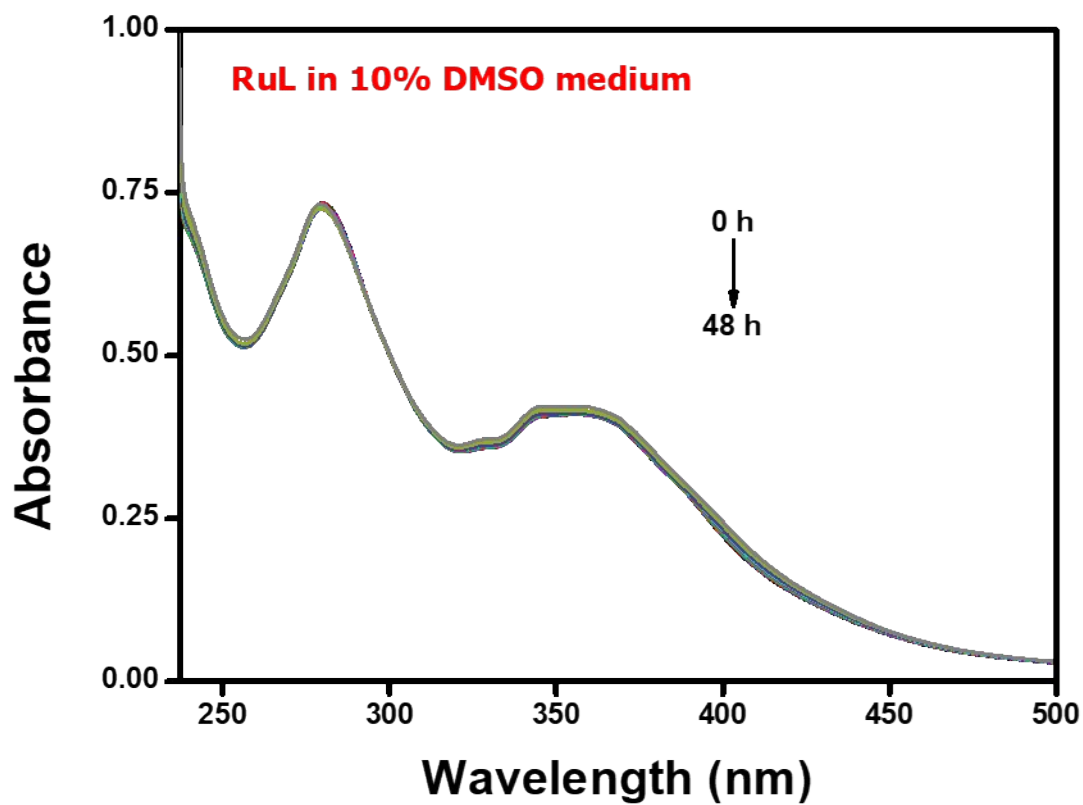


(b)

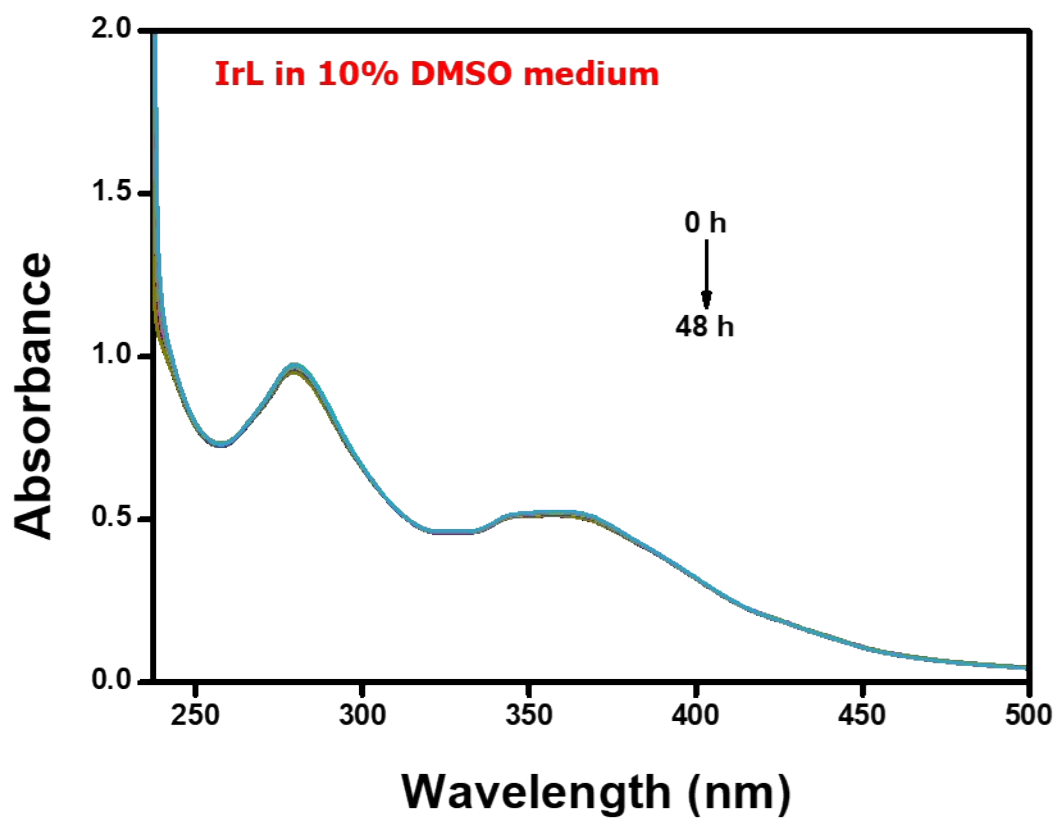


(c)

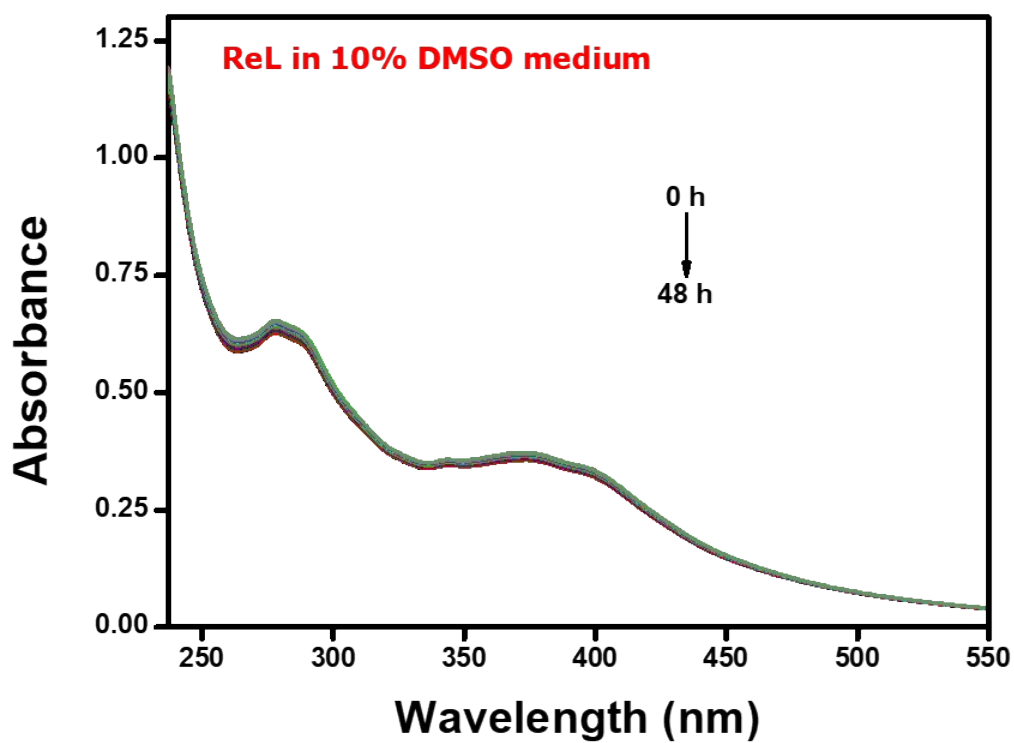
Fig. S4: Stability study of (a) RuL, (b) IrL, (c) ReL complexes in GSH medium



(a)

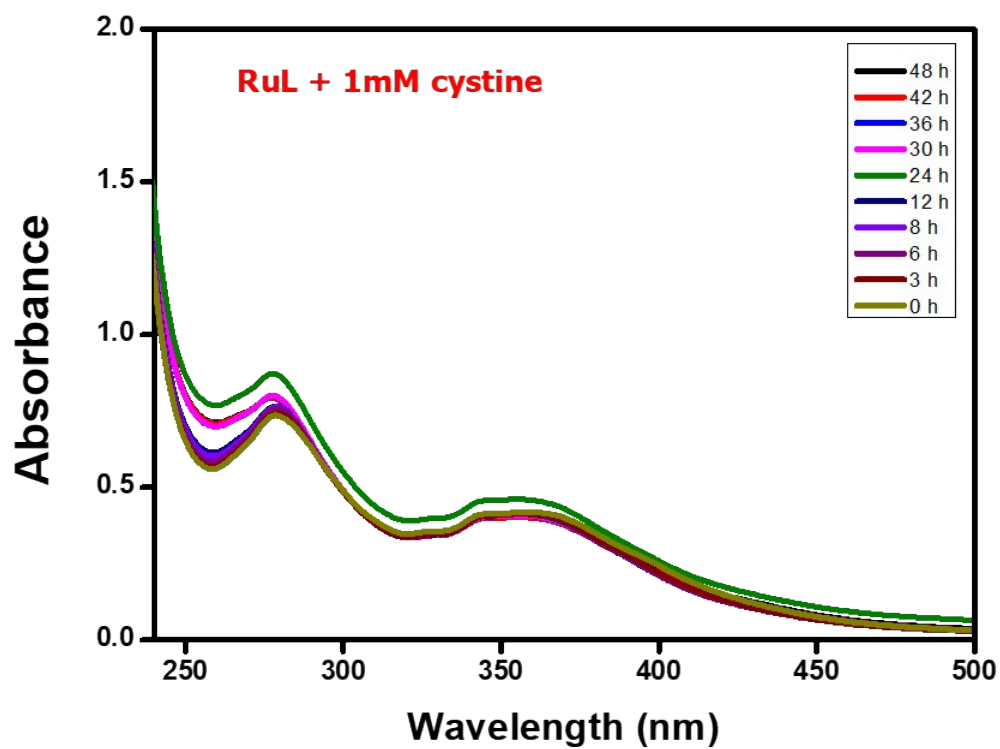


(b)

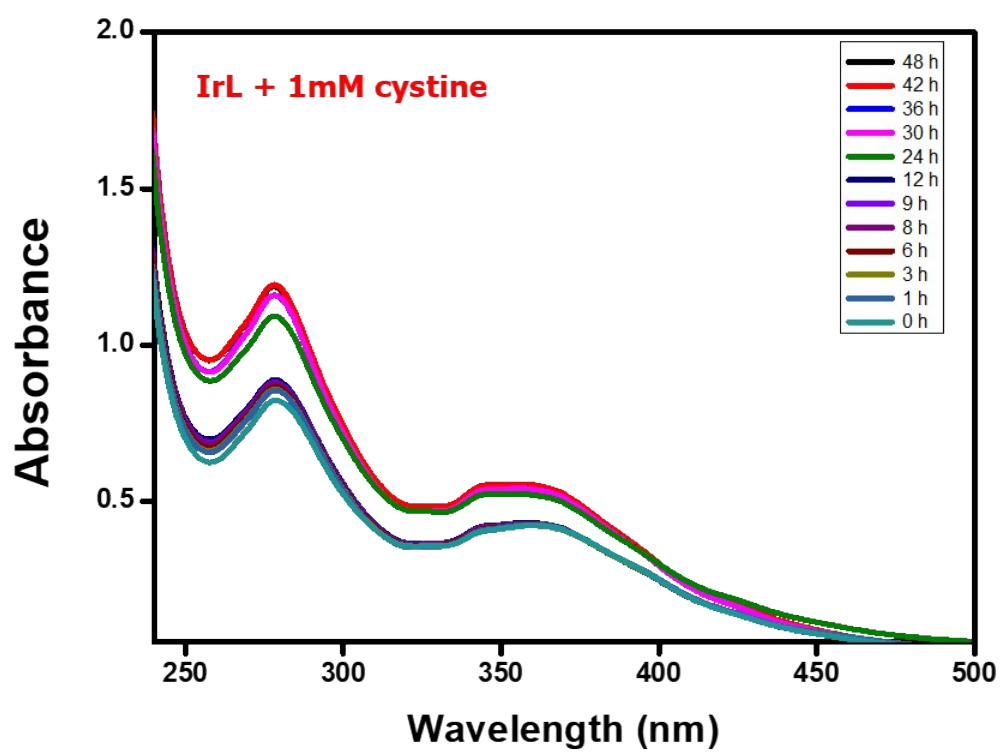


(c)

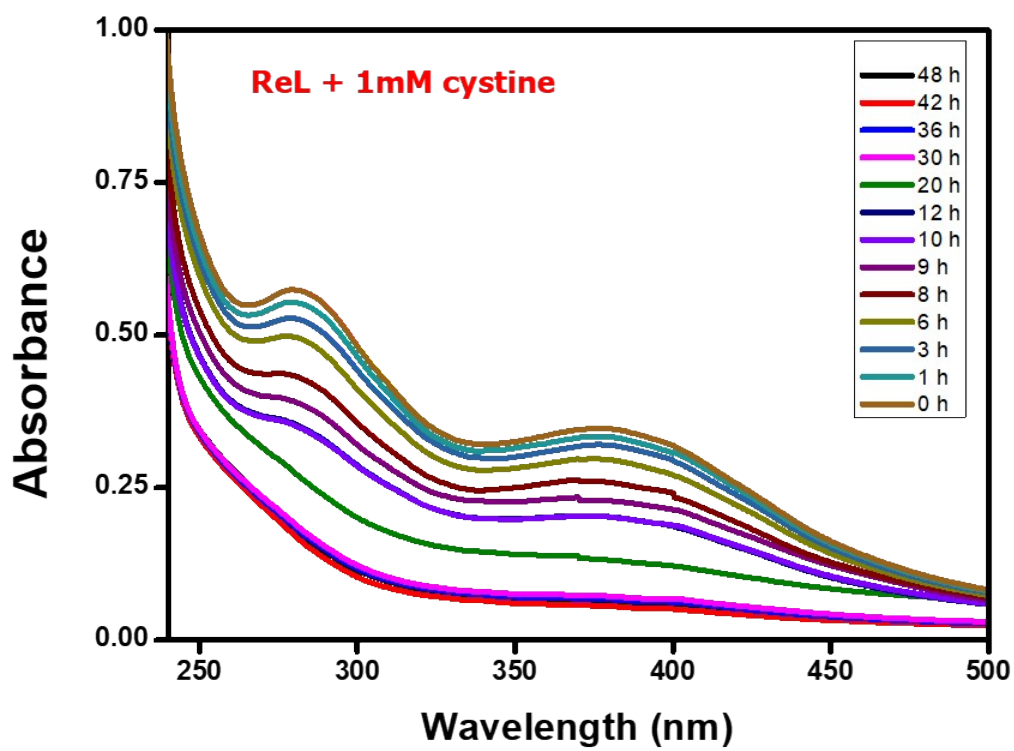
Fig. S5: Stability study of (a) RuL, (b) IrL, and (c) ReL complexes in 10% DMSO



(a)

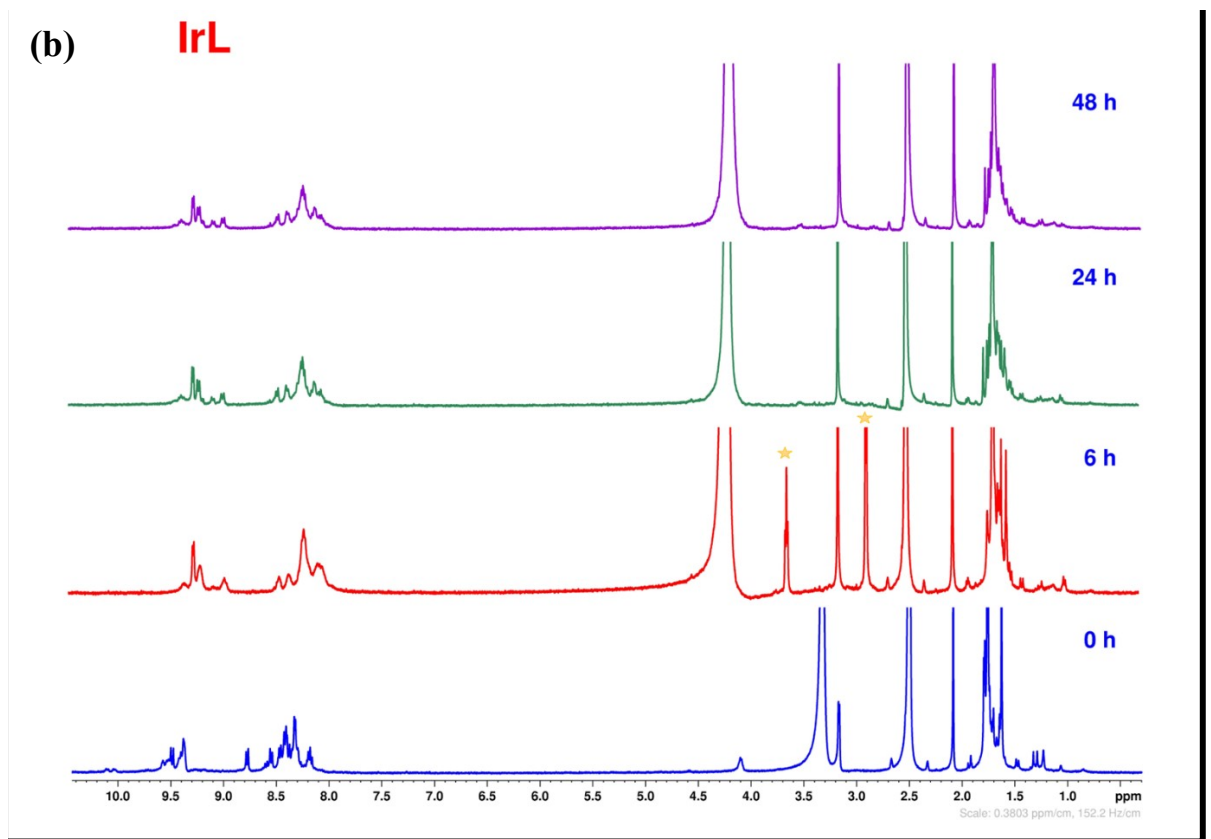
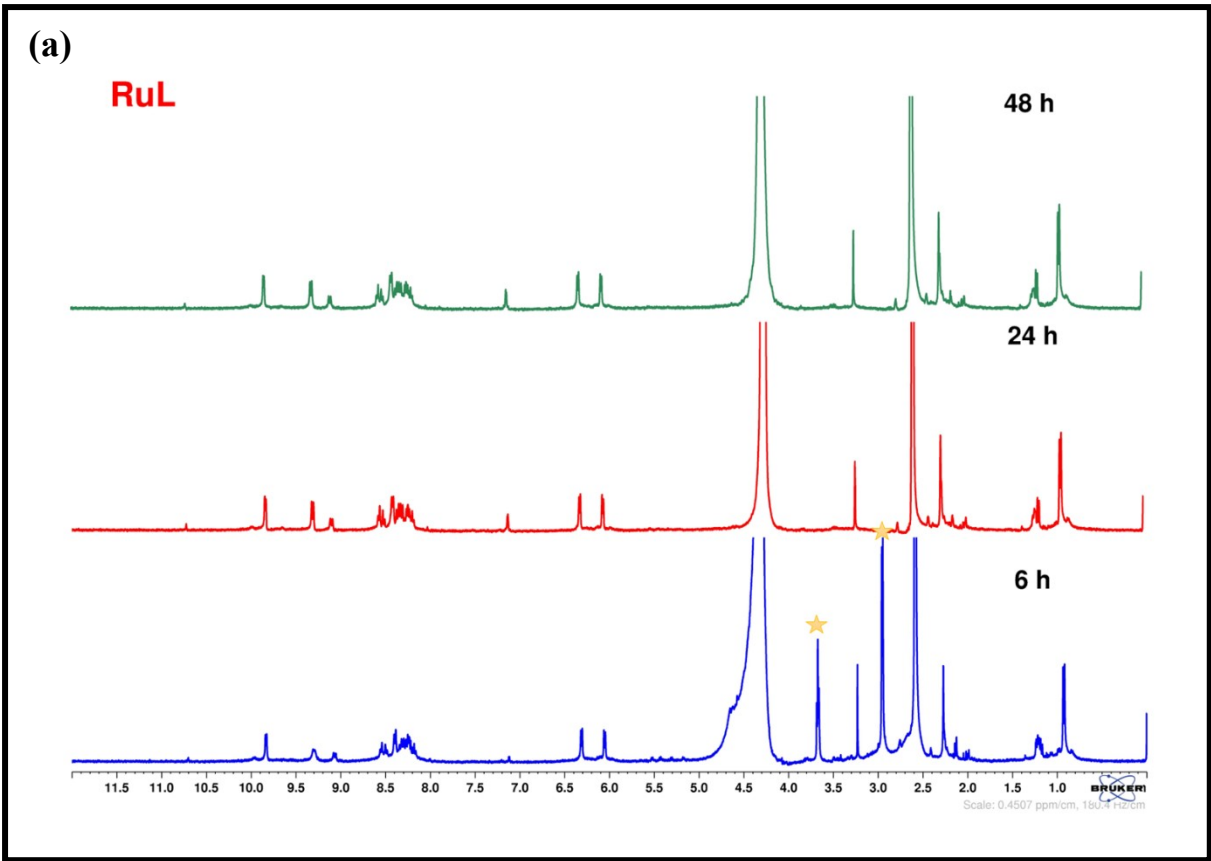


(b)



(c)

**Fig. S6: Stability study of (a) RuL, (b) IrL, (c) ReL complexes in presence of cystine**



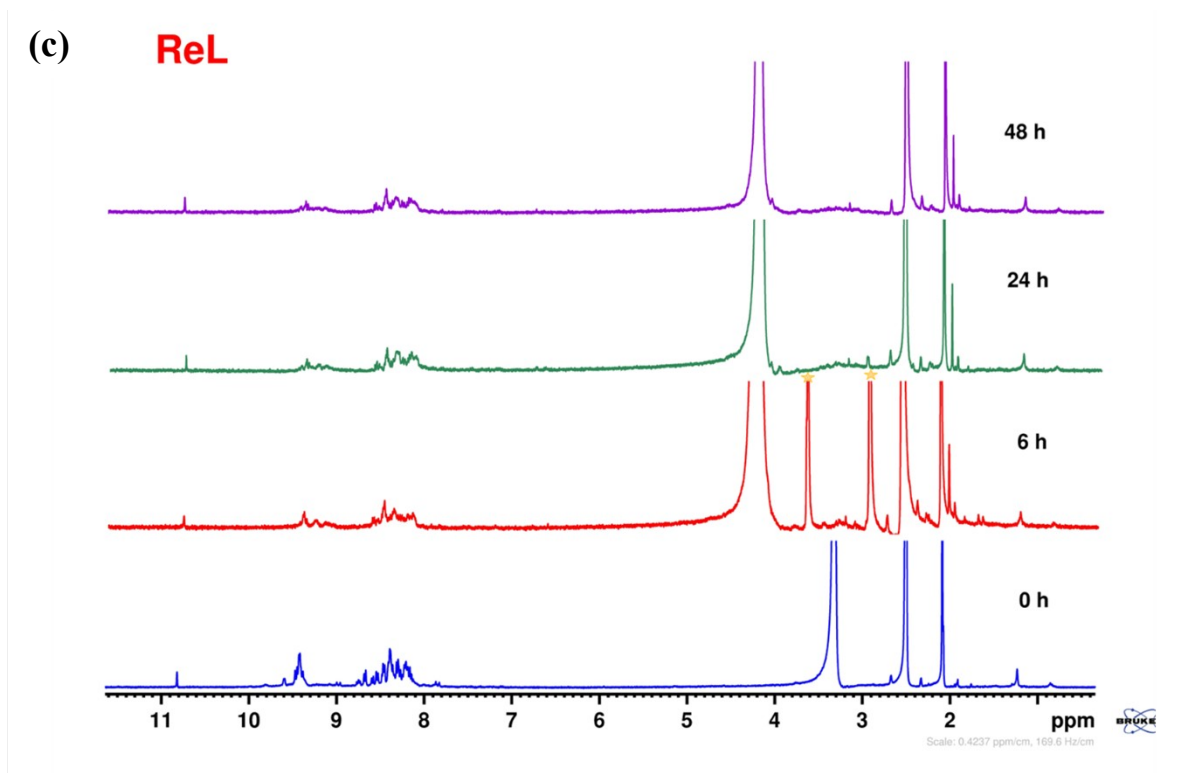
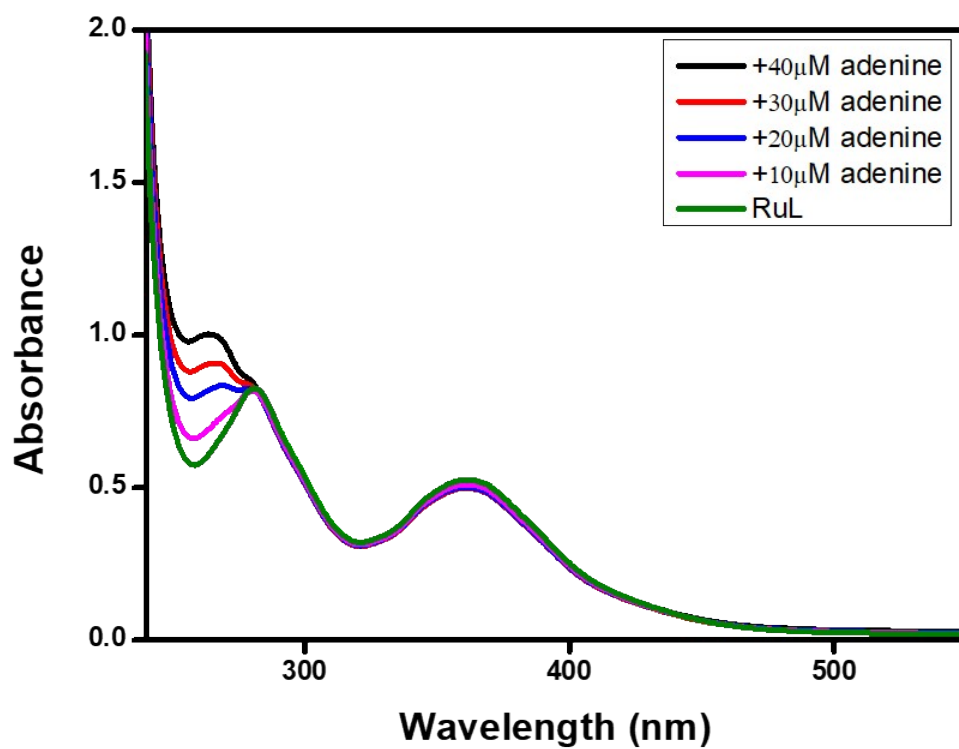
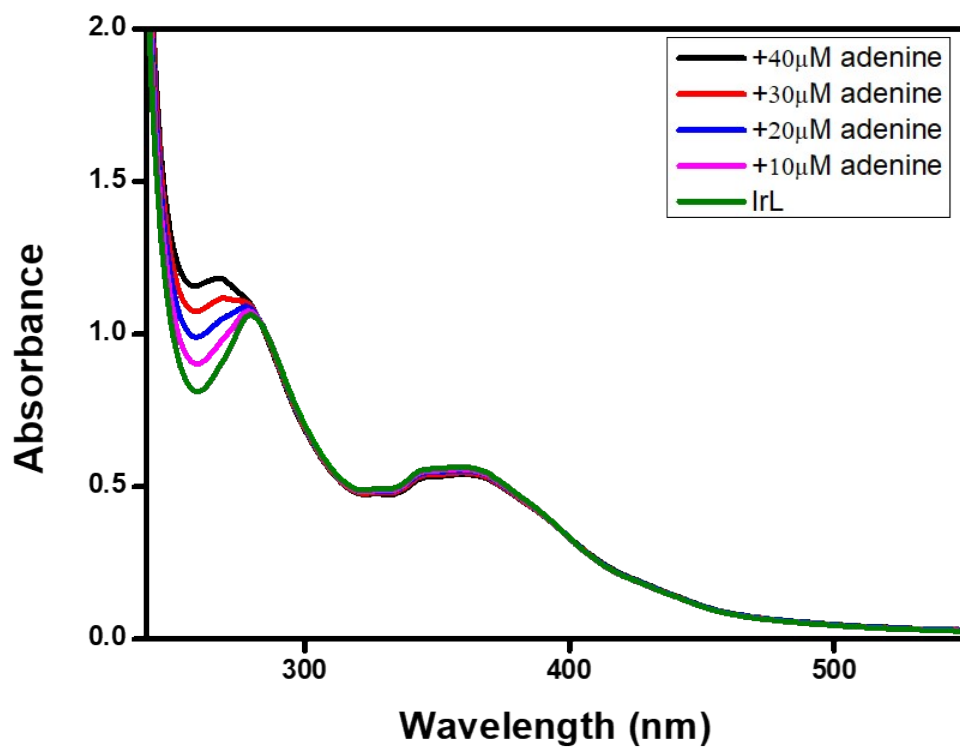


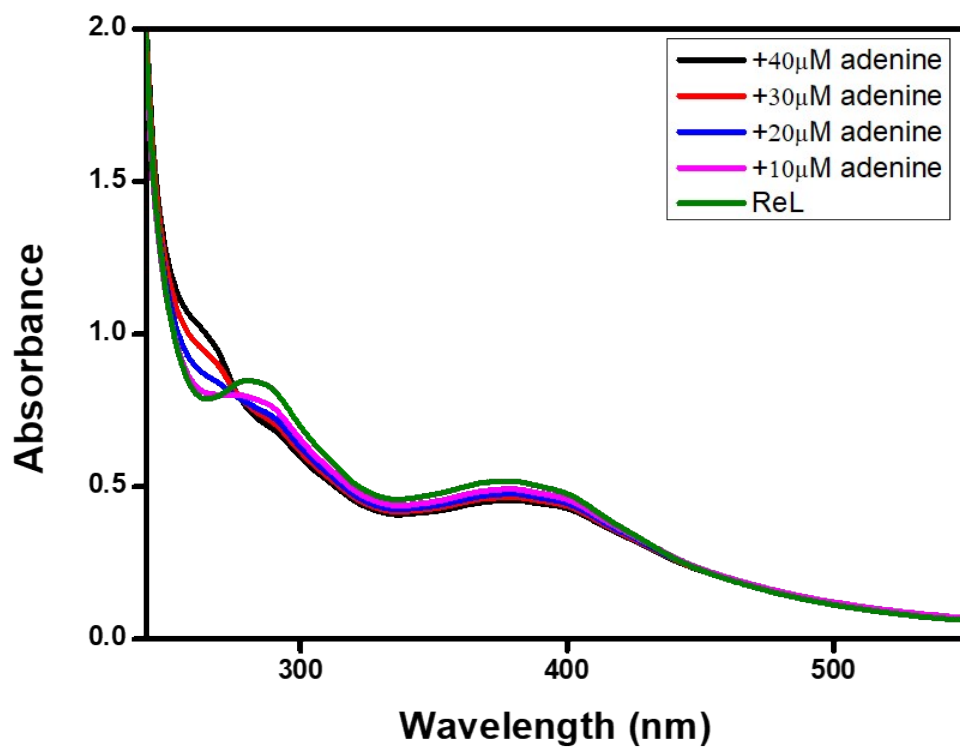
**Fig. S7:  $^1\text{H}$  NMR spectroscopic study on the stability of (a) RuL, (b) IrL, (c) ReL complexes in presence of cystine**



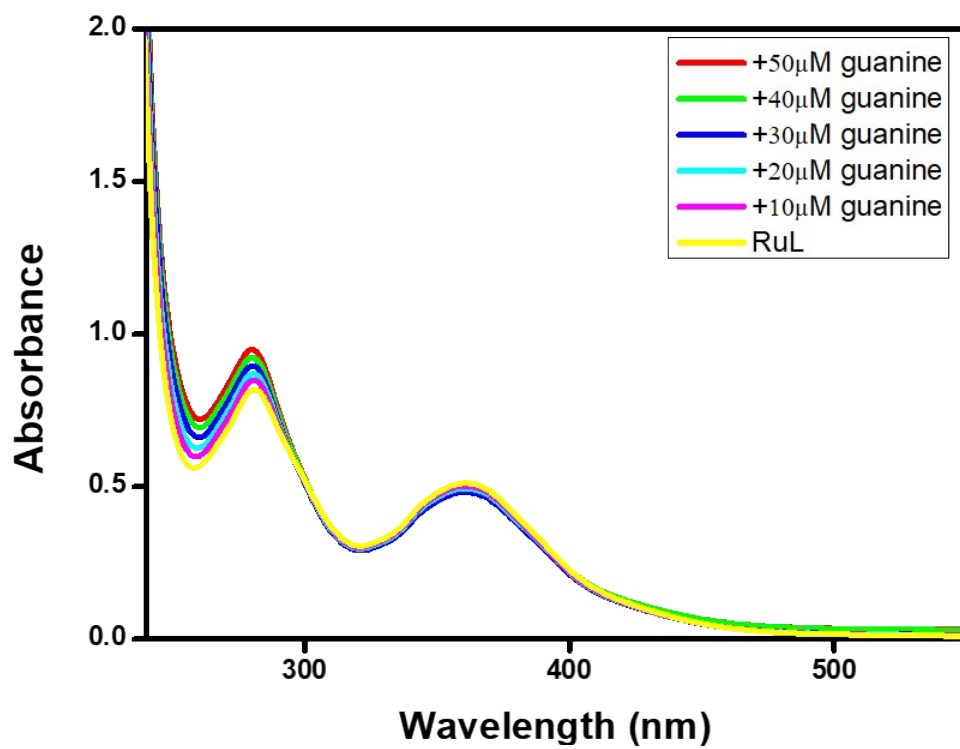
(a)



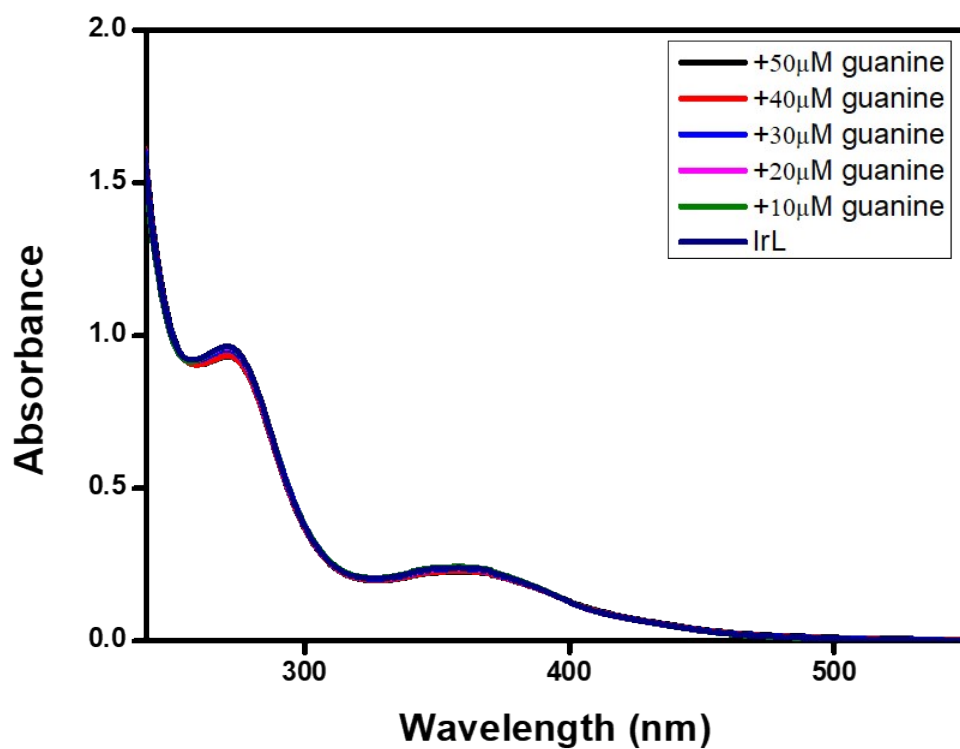
(b)



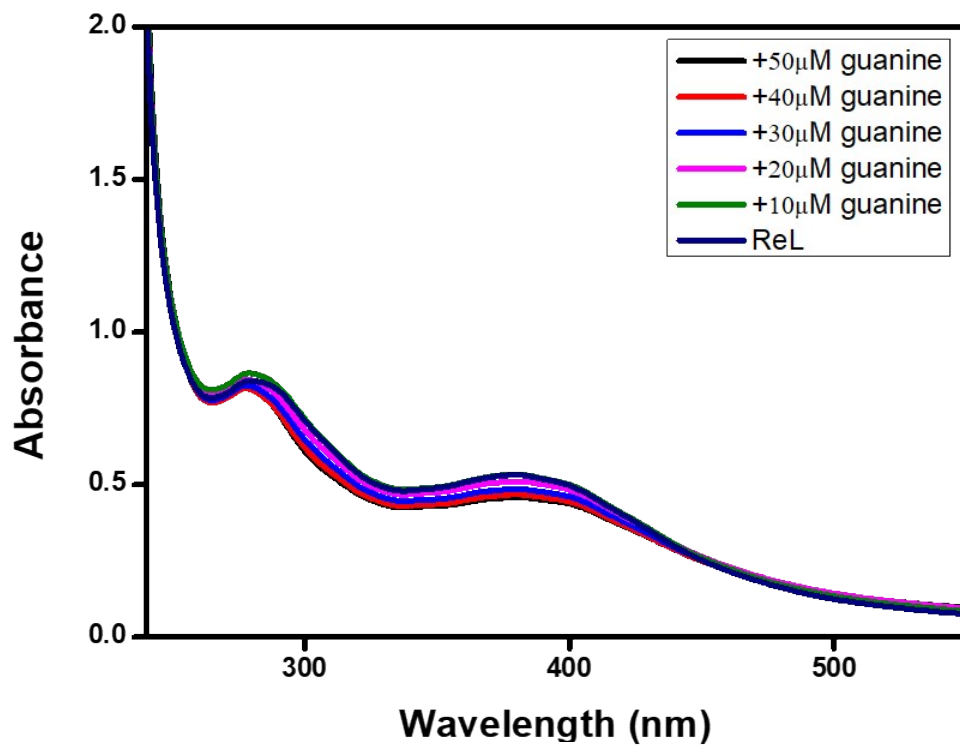
(c)



(d)

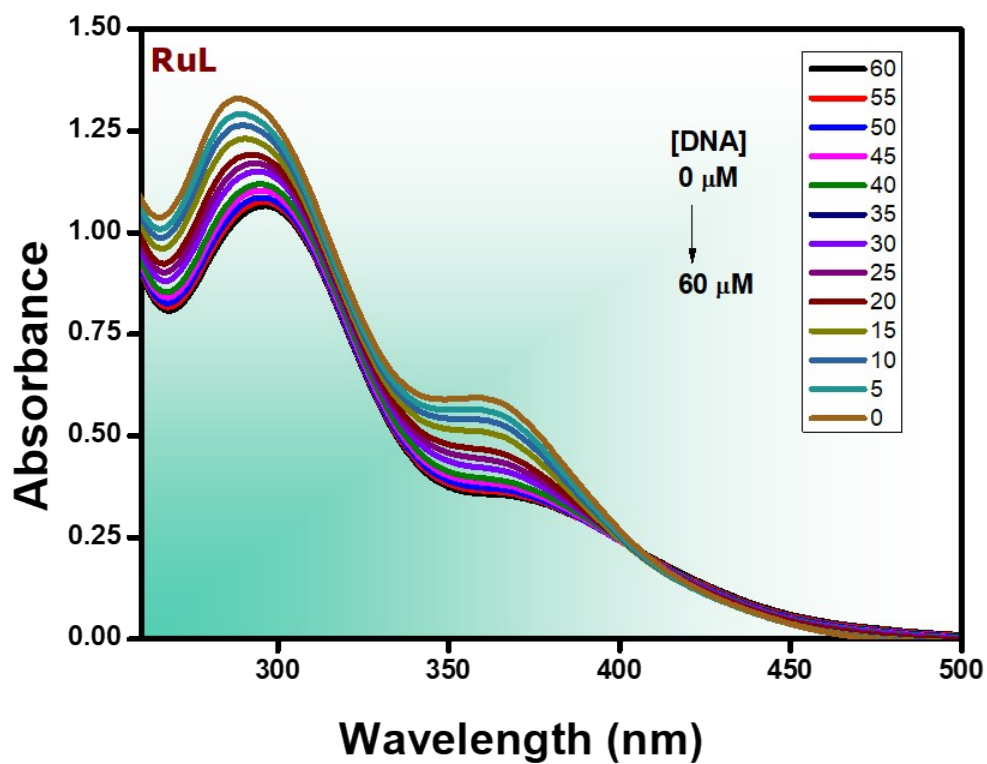


(e)

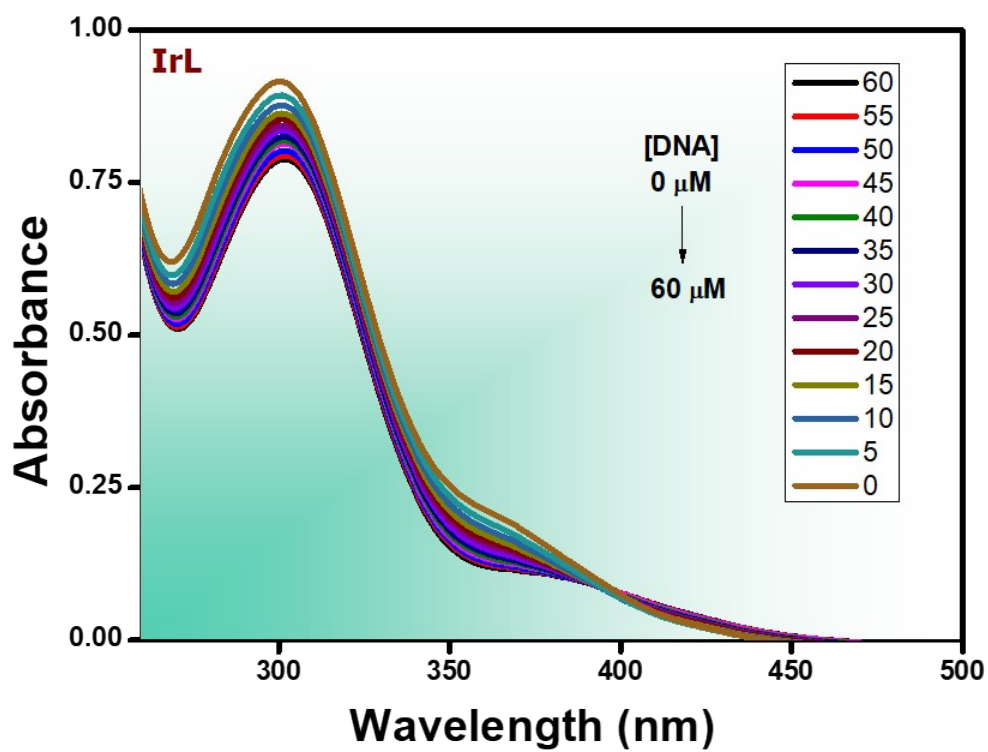


(f)

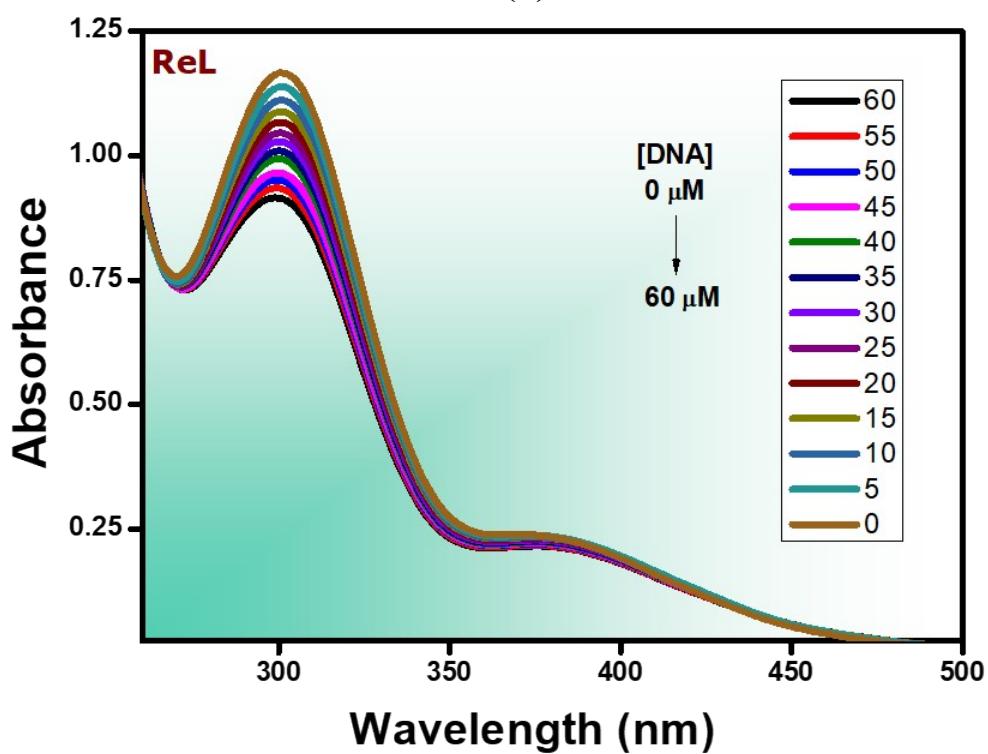
Fig. S8: Interaction of complexes RuL, IrL, & ReL with adenine (a,b,c) and guanine (d,e,f)



(a)

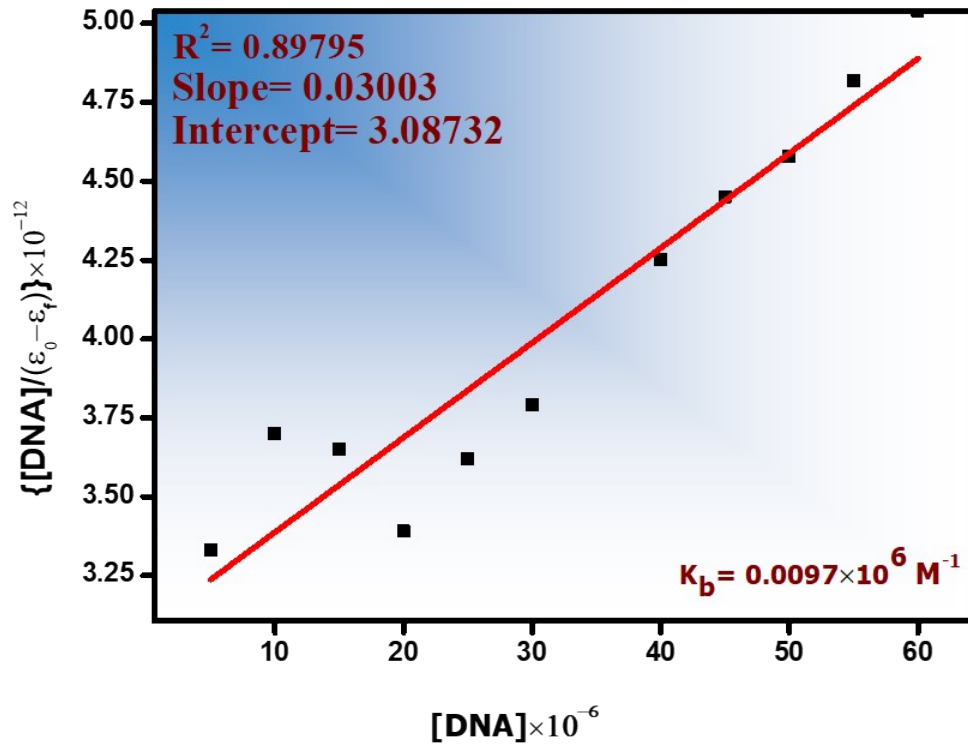


(b)

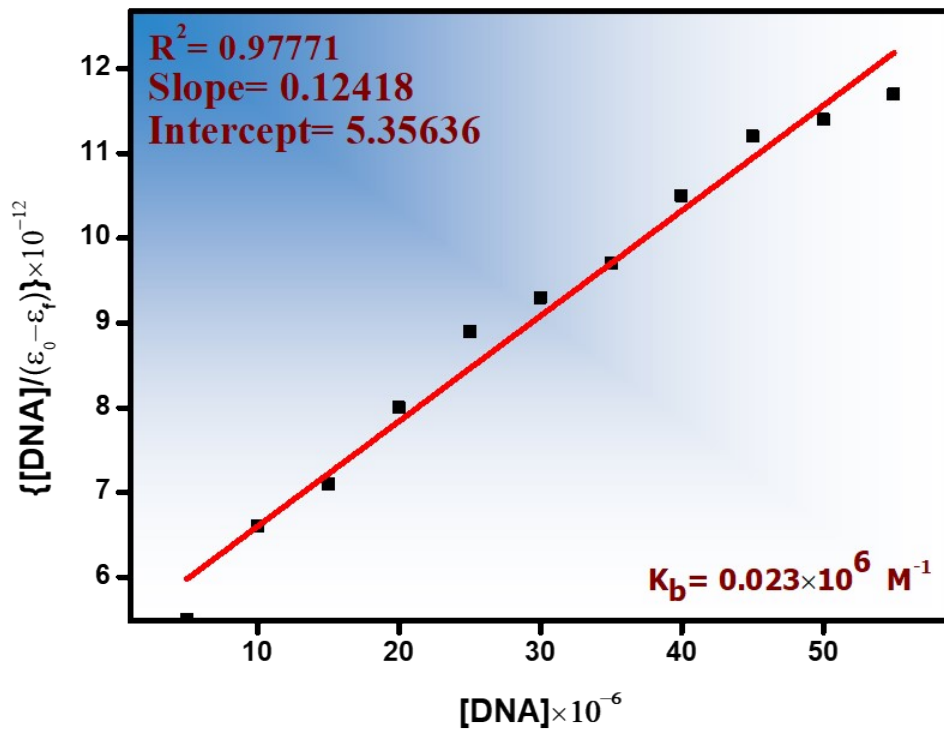


(c)

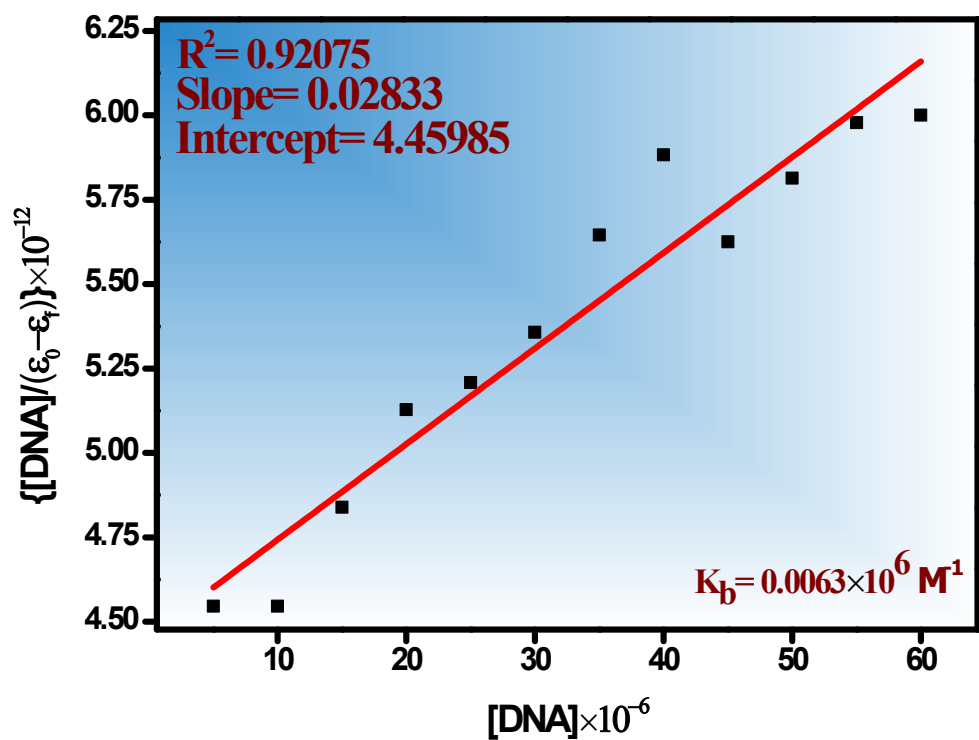
Fig. S9: DNA binding plot of (a) RuL (b) IrL and (c) ReL complexes



(a)

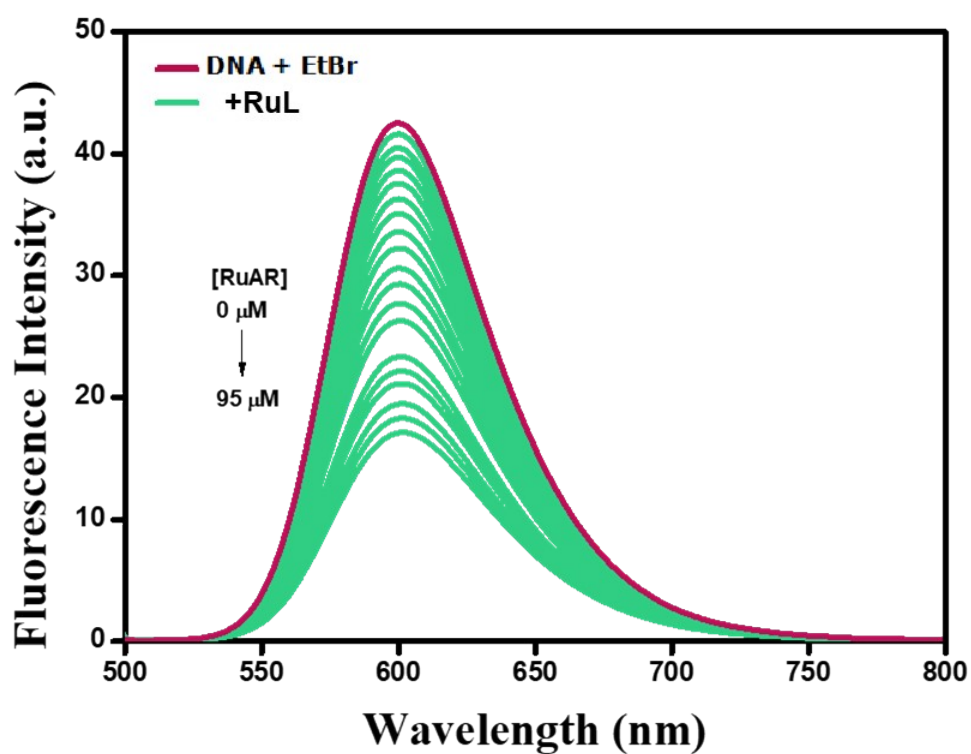


(b)

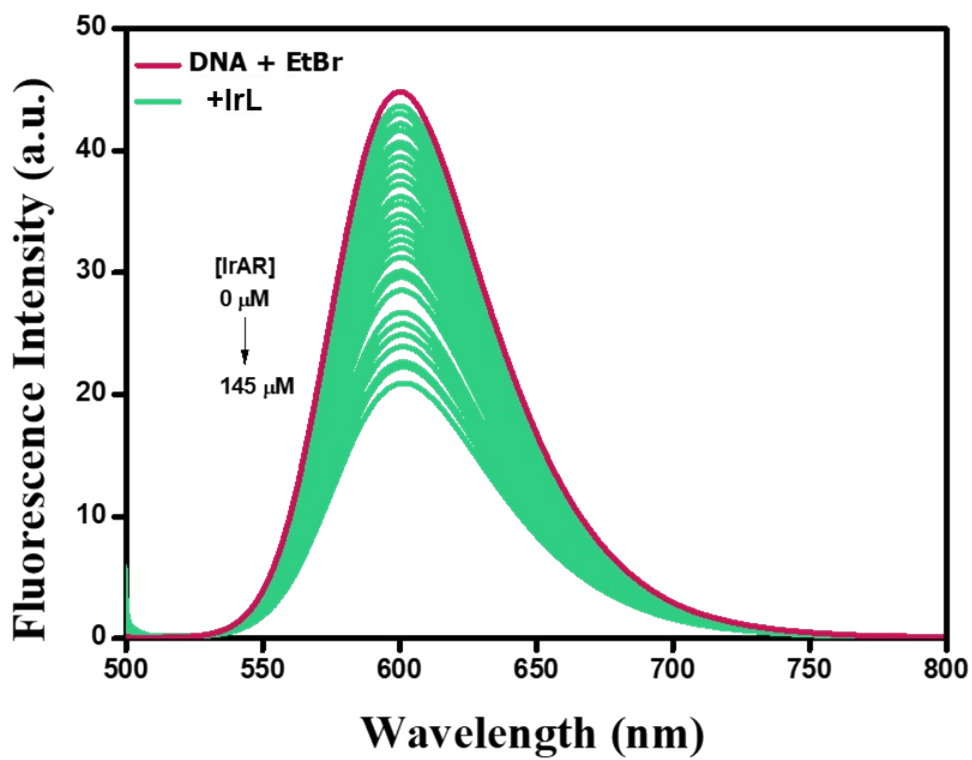


(c)

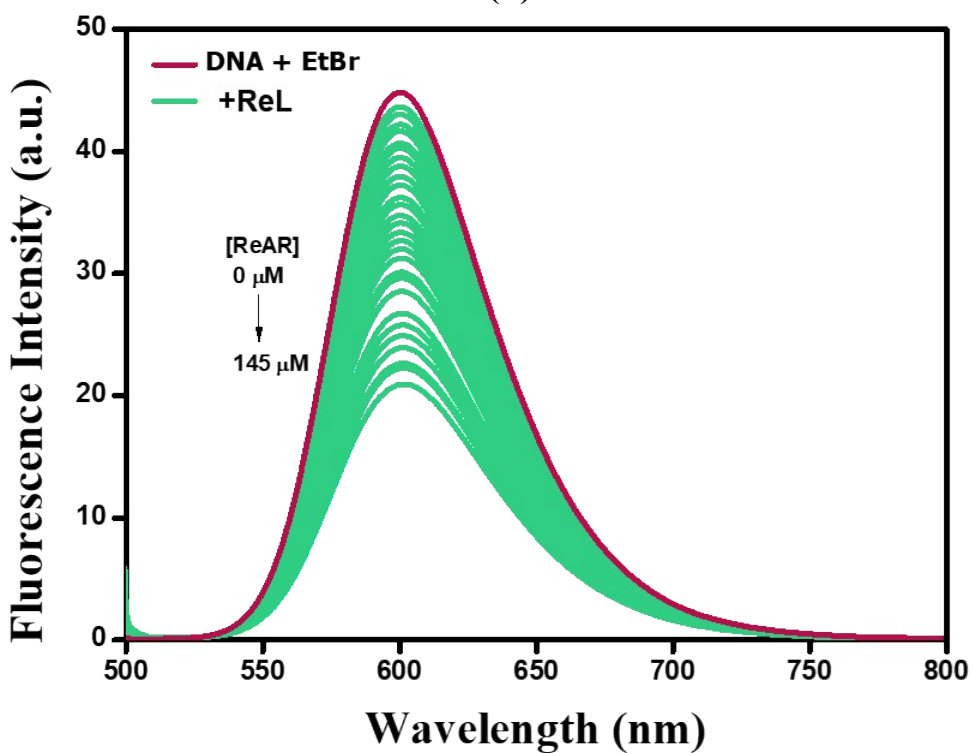
Fig. S10:  $\{[DNA]/\epsilon_0-\epsilon_f\} \times 10^{-12}$  vs.  $[DNA]$  linear plot of complex (a) RuL (b) IrL and (c) ReL



(a)

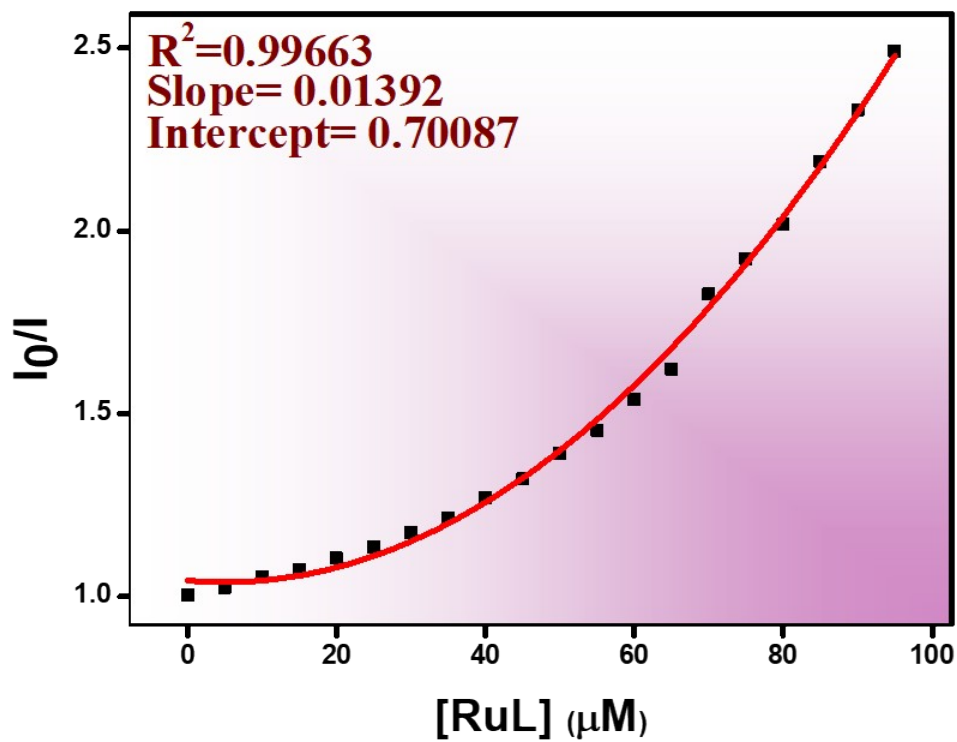


(b)

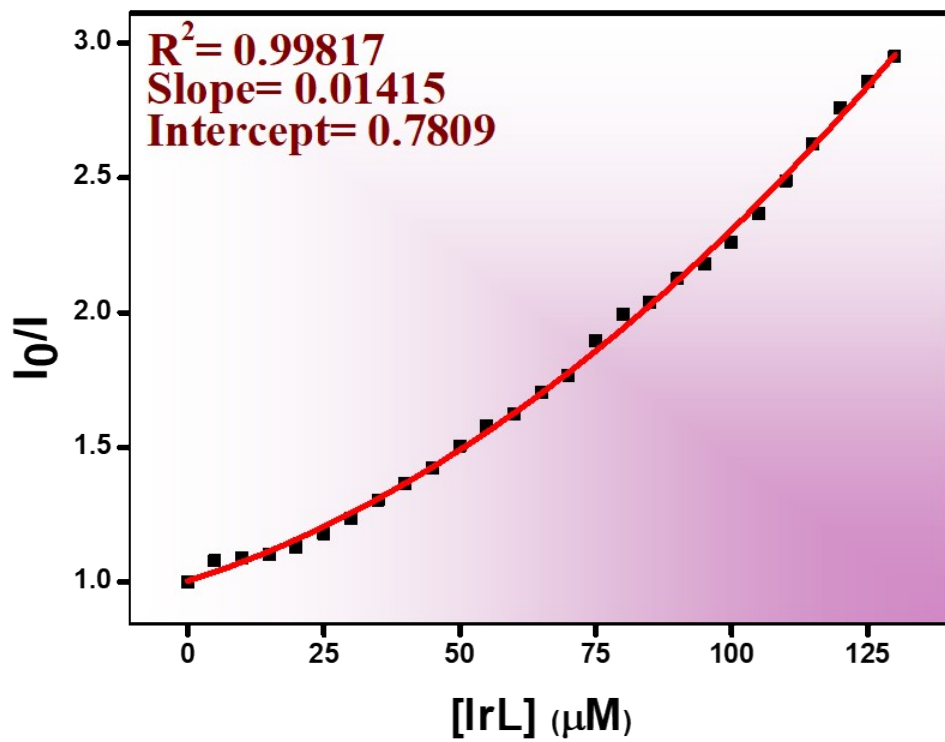


(c)

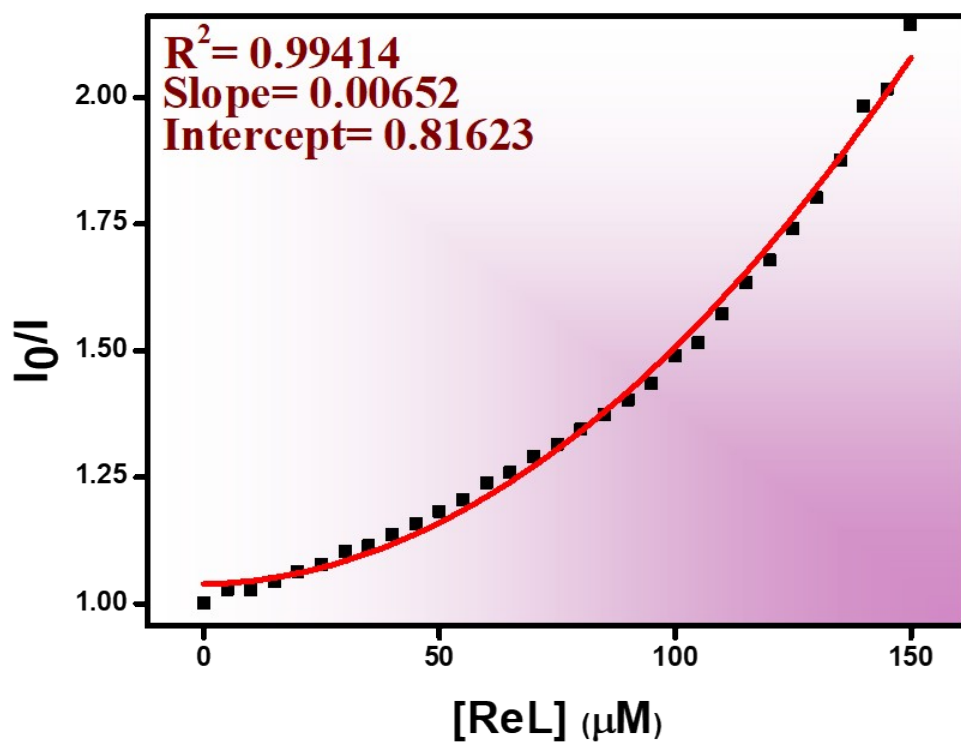
Fig. S11: Plot of fluorescence quenching EtBr-DNA with increasing complexes (a) RuL (b) IrL (c) ReL



(a)



(b)



(c)

Fig. S12: Stern-Volmer plot  $I_0/I$  vs. concentration of complex (a) RuL (b) IrL and (c) ReL.

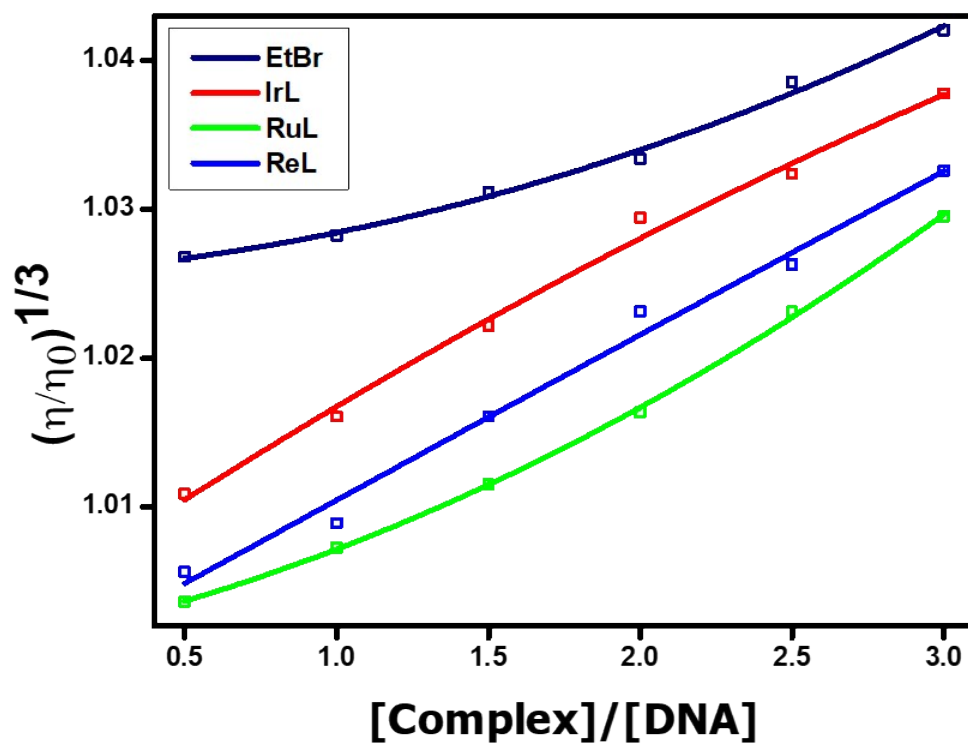
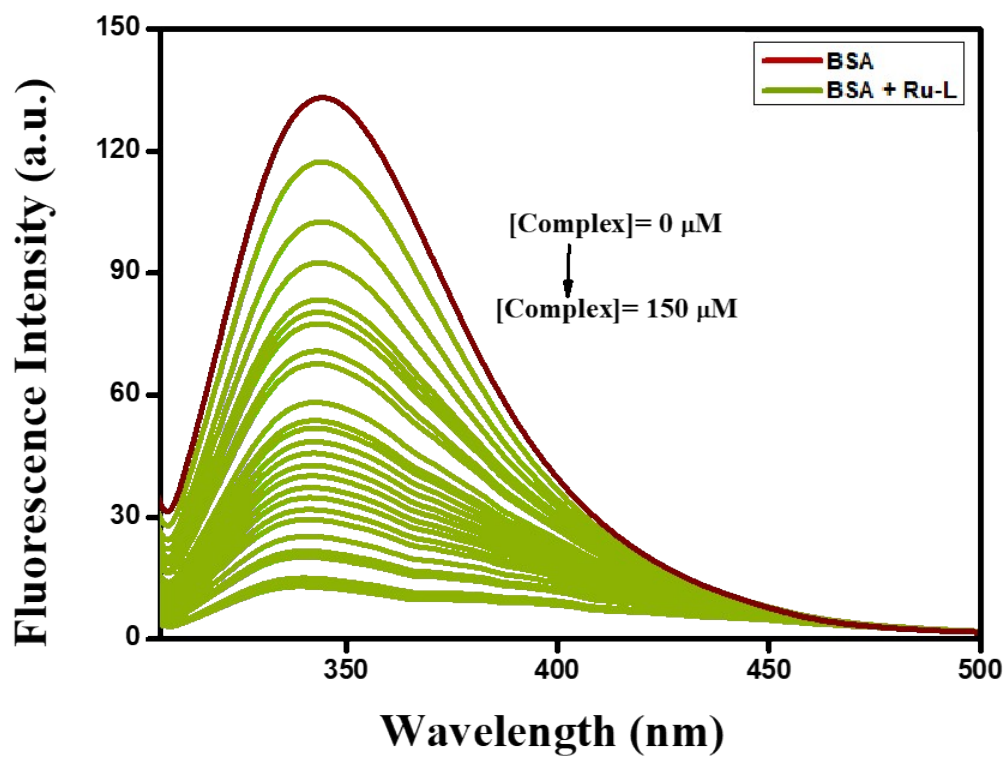
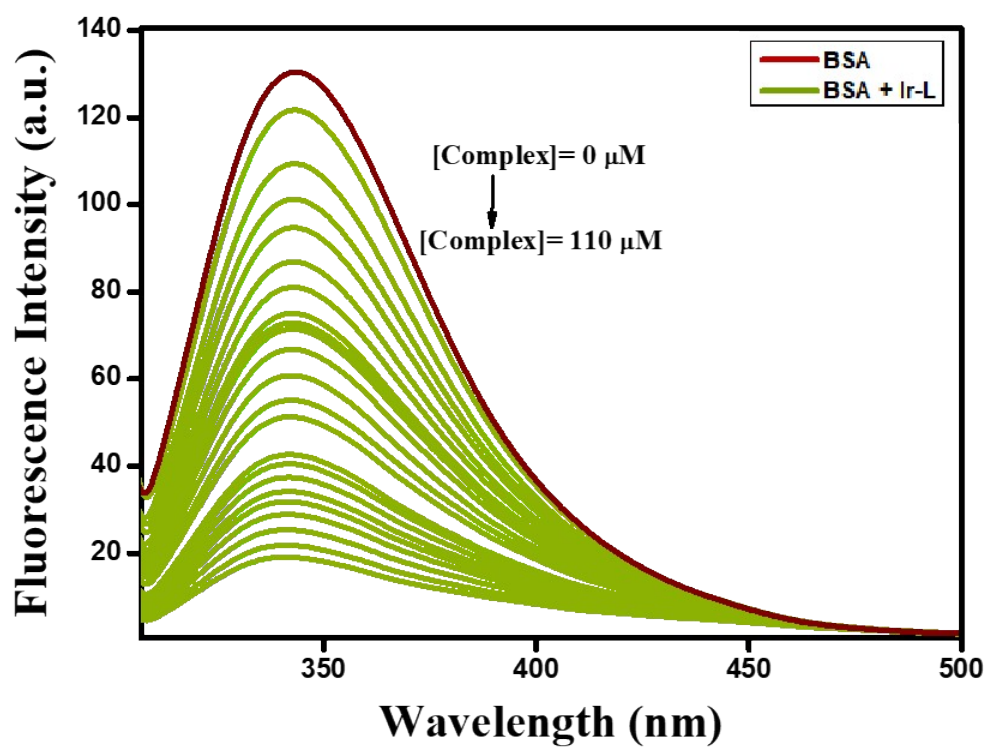


Fig. S13: Relative viscosity plot of ct-DNA with RuL, IrL, ReL with respect to EtBr



(a)



(b)

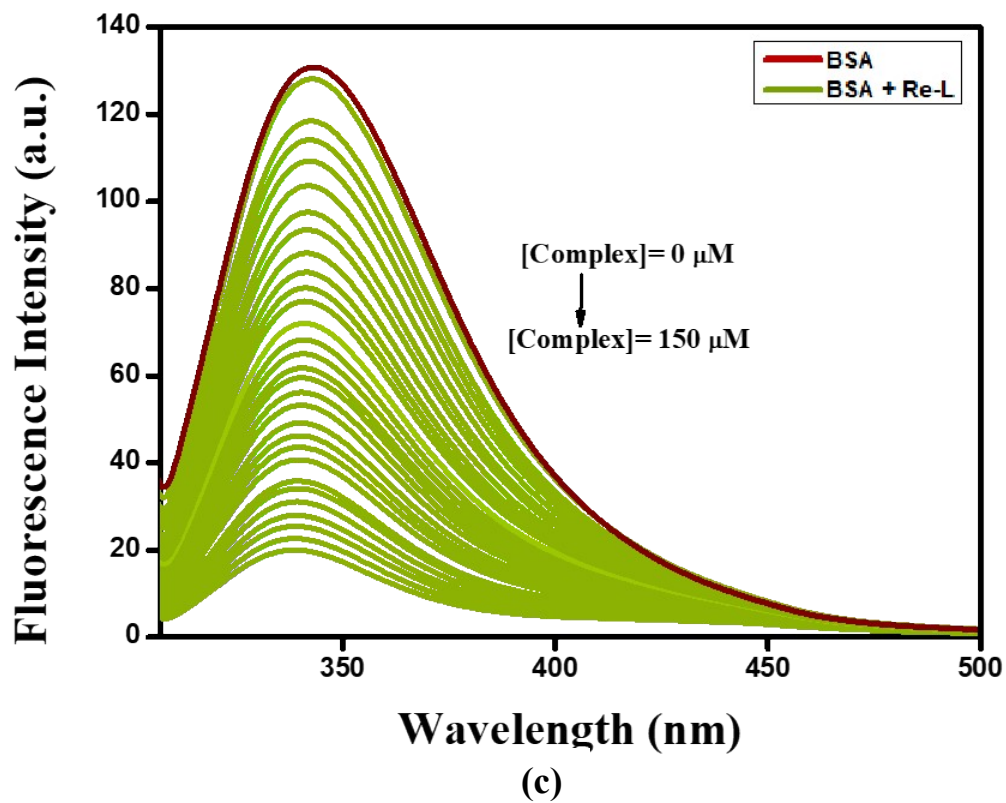
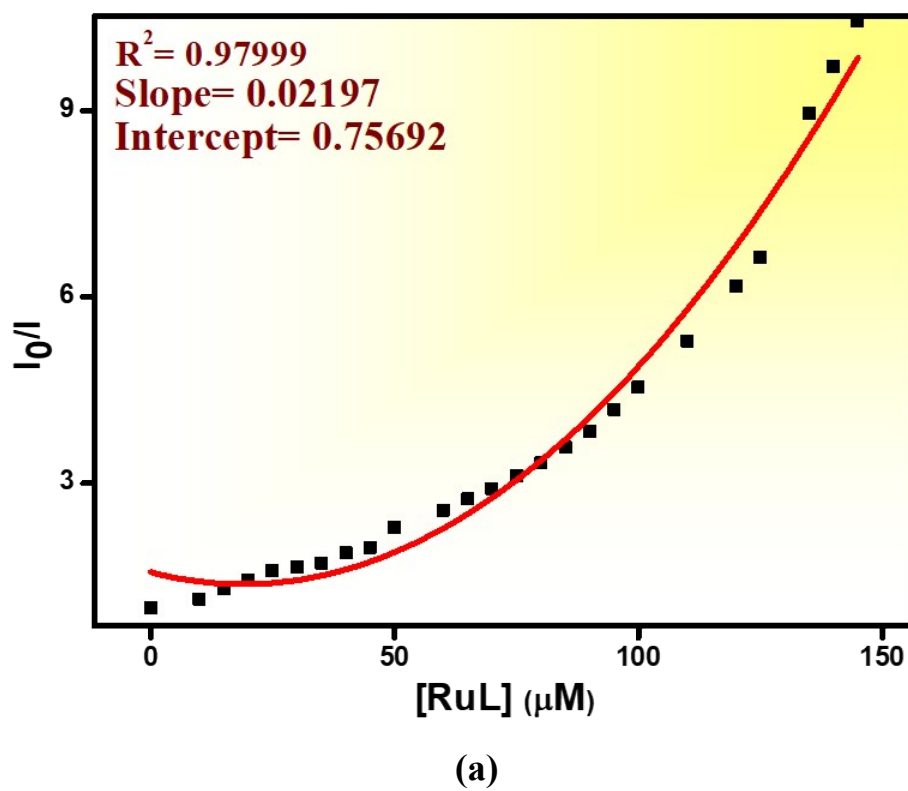
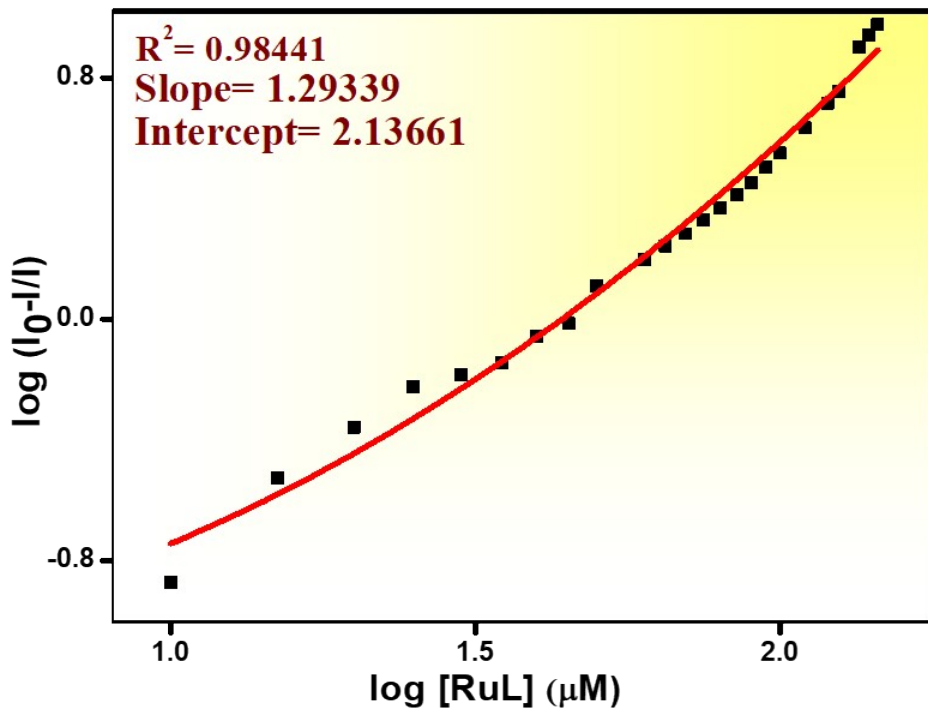
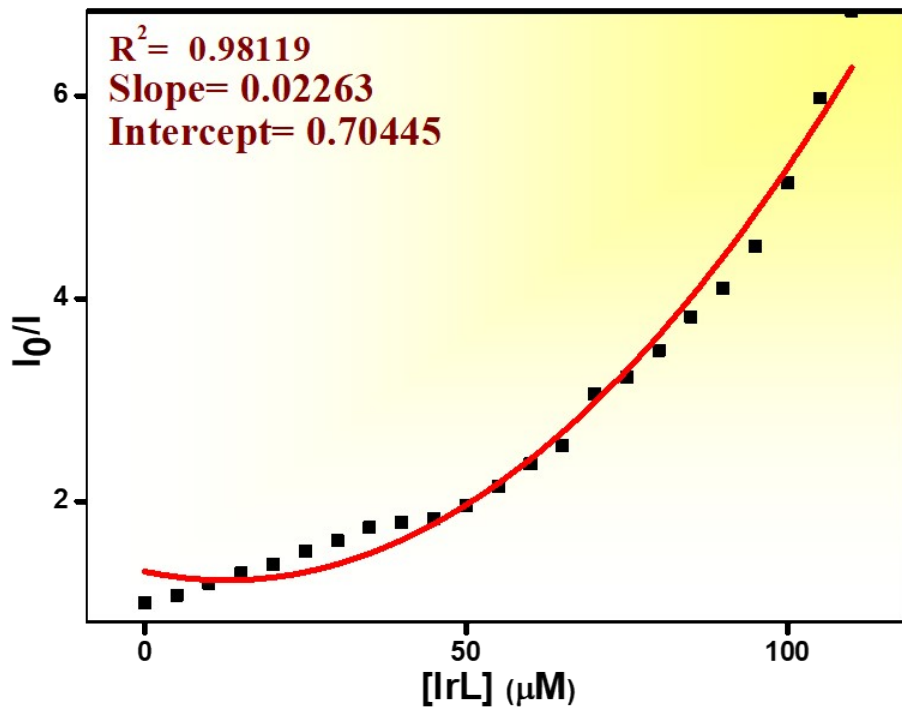


Fig. S14: Interaction of complex (a) RuL (b) IrL (c) ReL with BSA

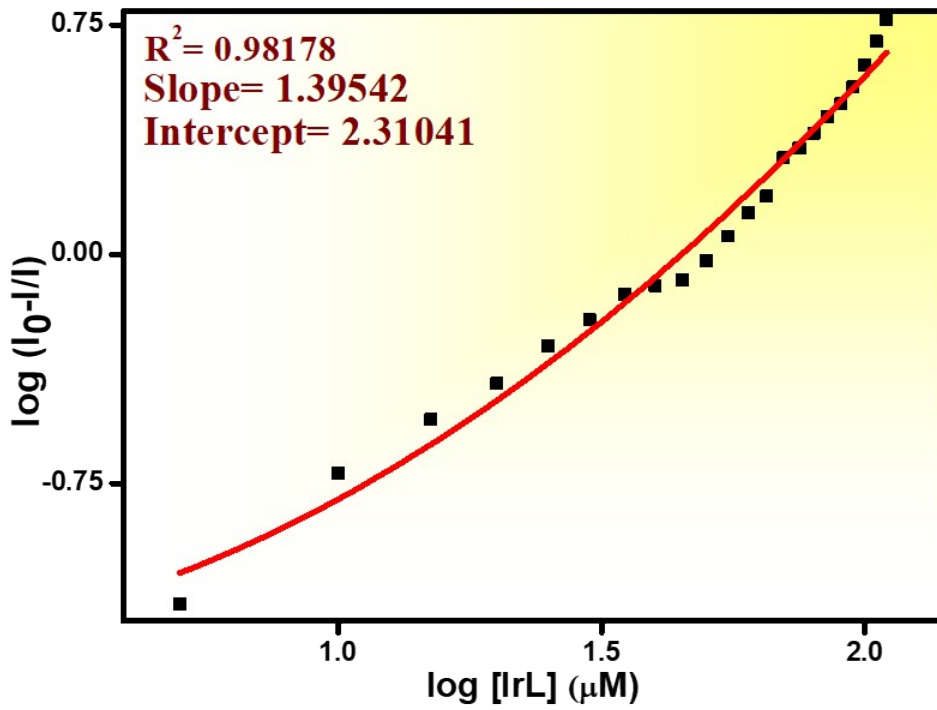




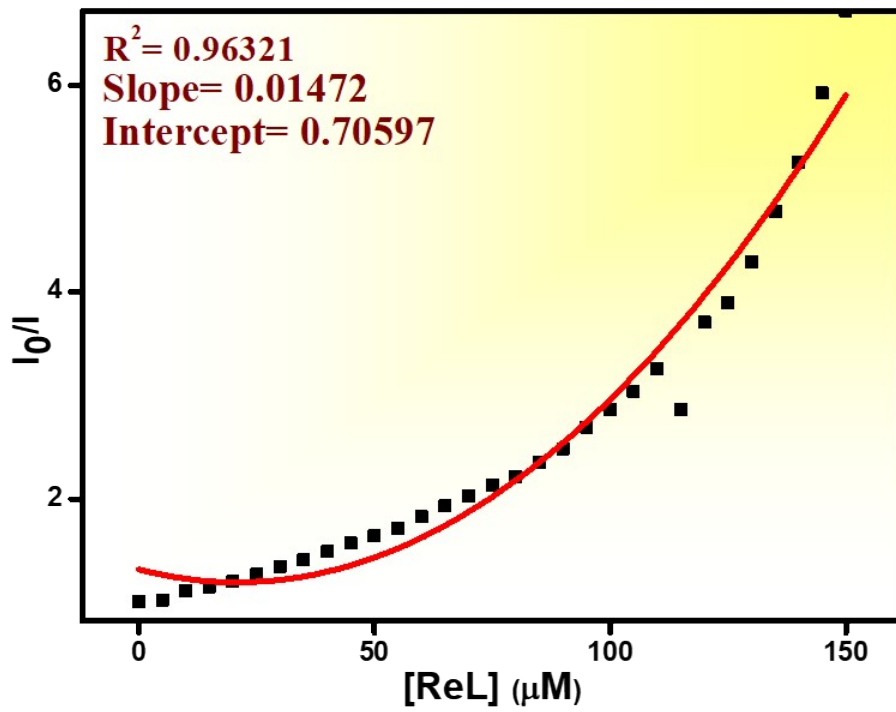
(b)



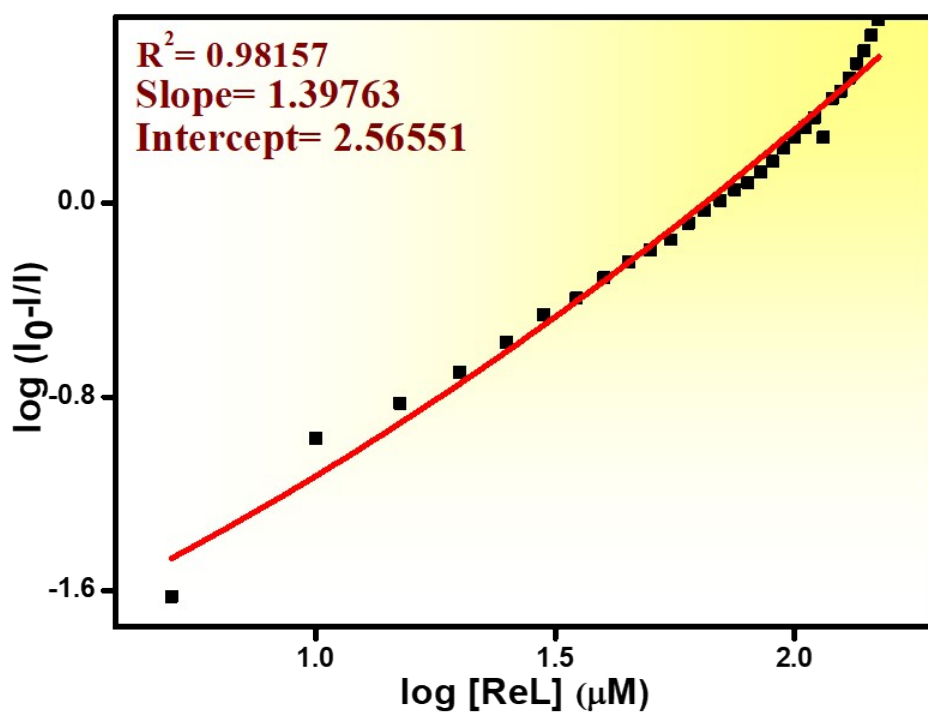
(c)



(d)

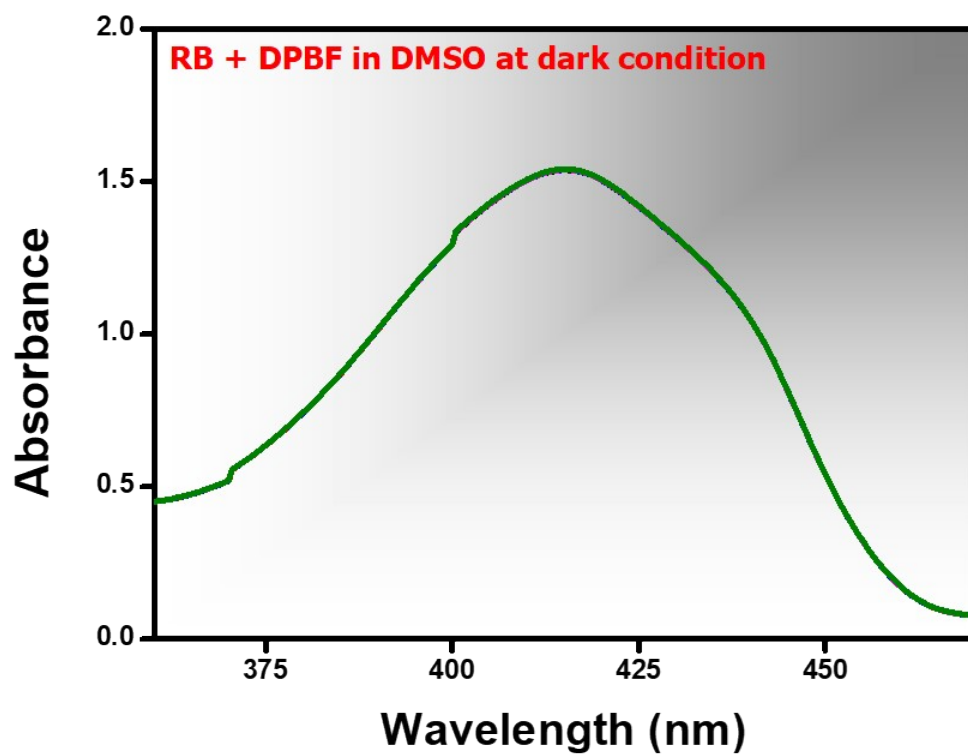


(e)

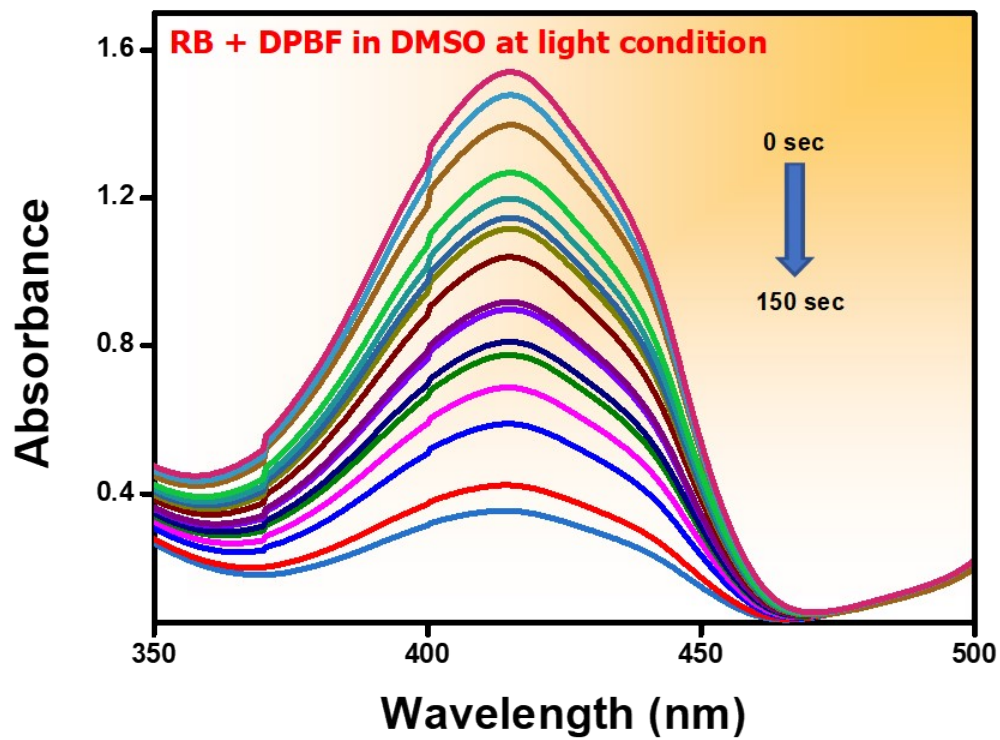


(f)

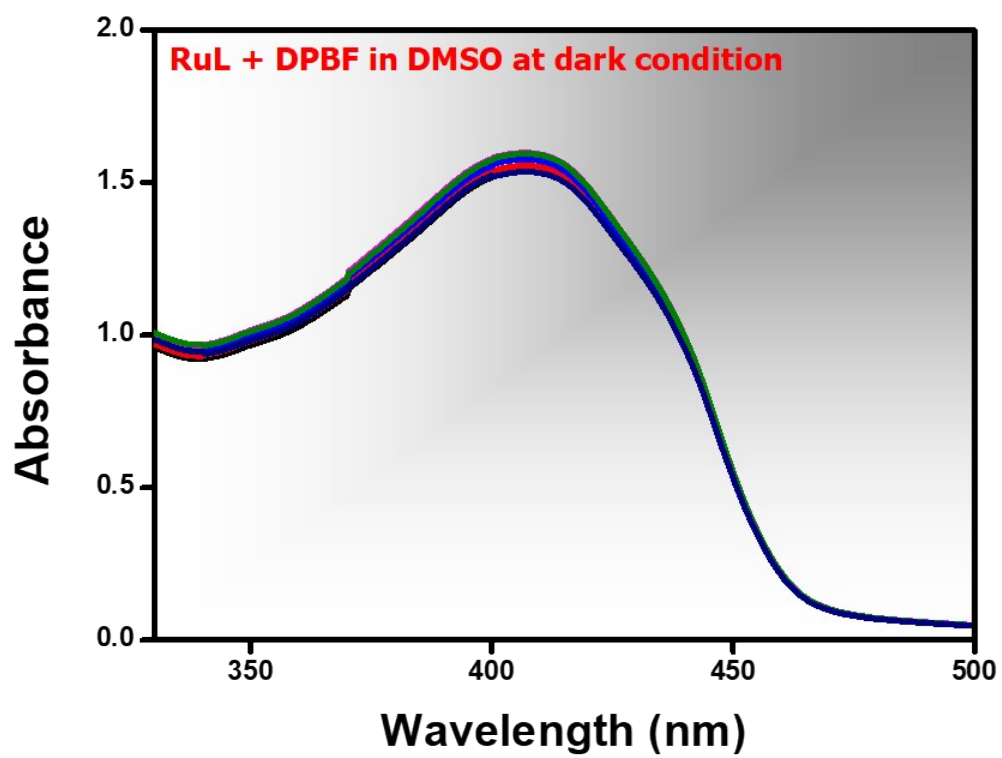
**Fig. S15: Stern-Volmer plot  $I_0/I$  vs. concentration of complex (a) RuL (c) IrL (e) ReL. Scatchard plot of  $\log [I_0 - I/I]$  vs.  $\log [\text{complex}]$  for BSA in presence of complex (b) RuL (d) IrL (f) ReL**



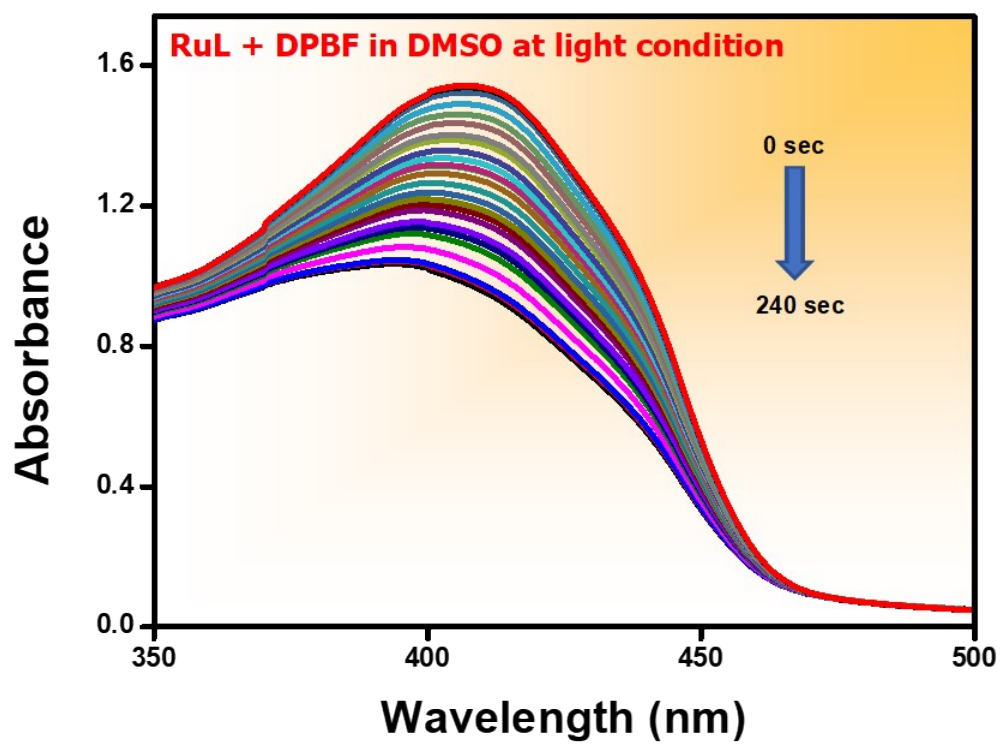
(a)



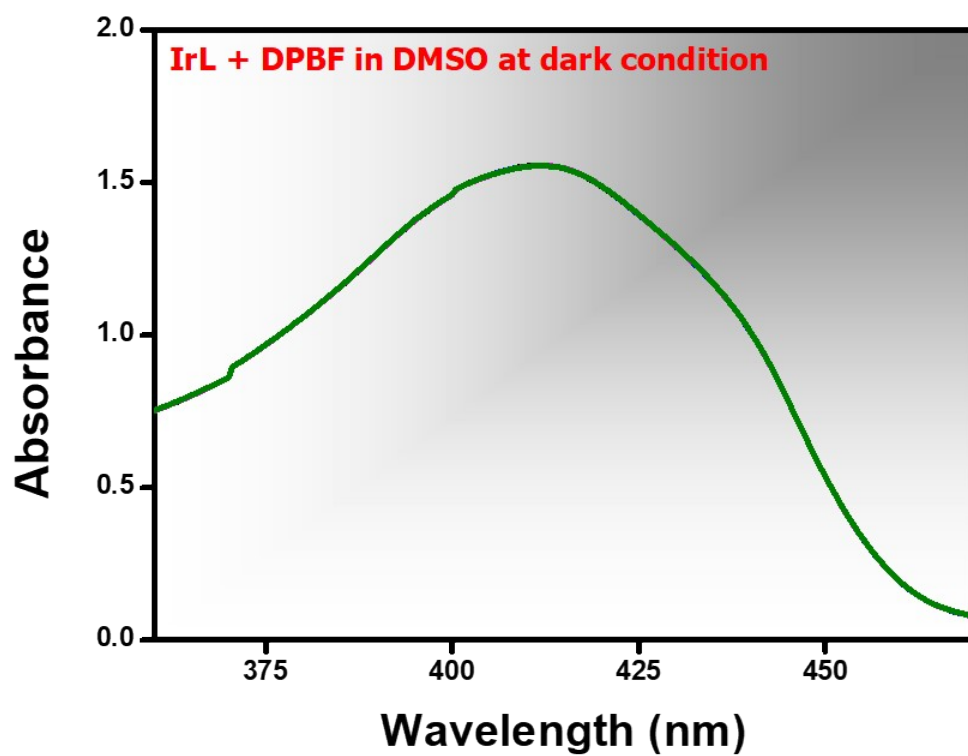
(b)



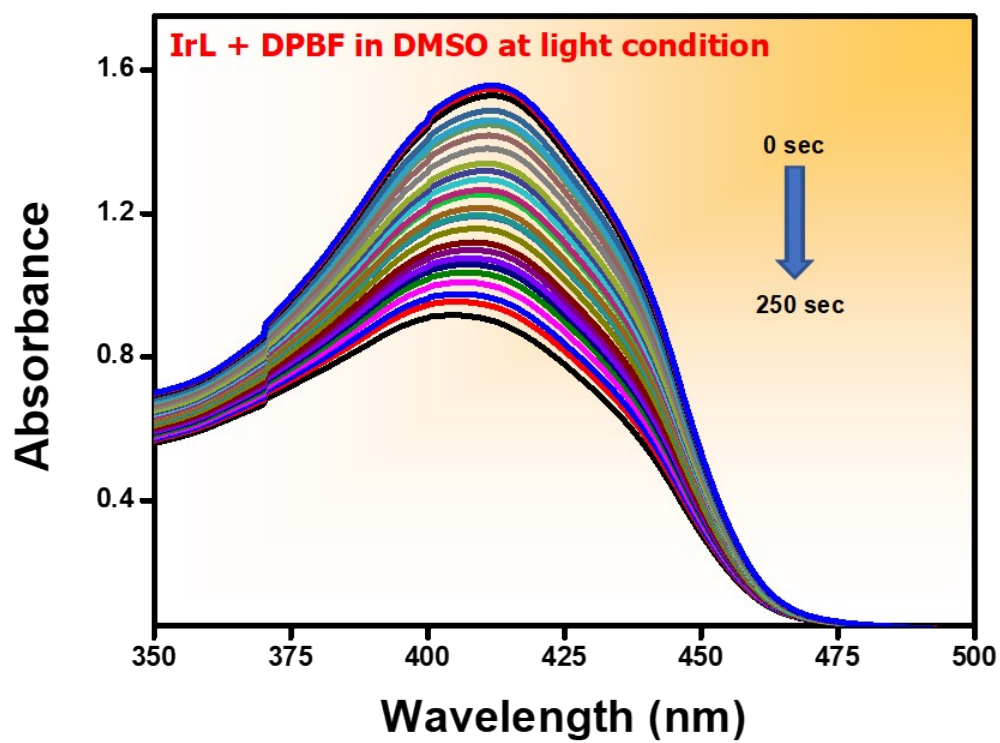
(c)



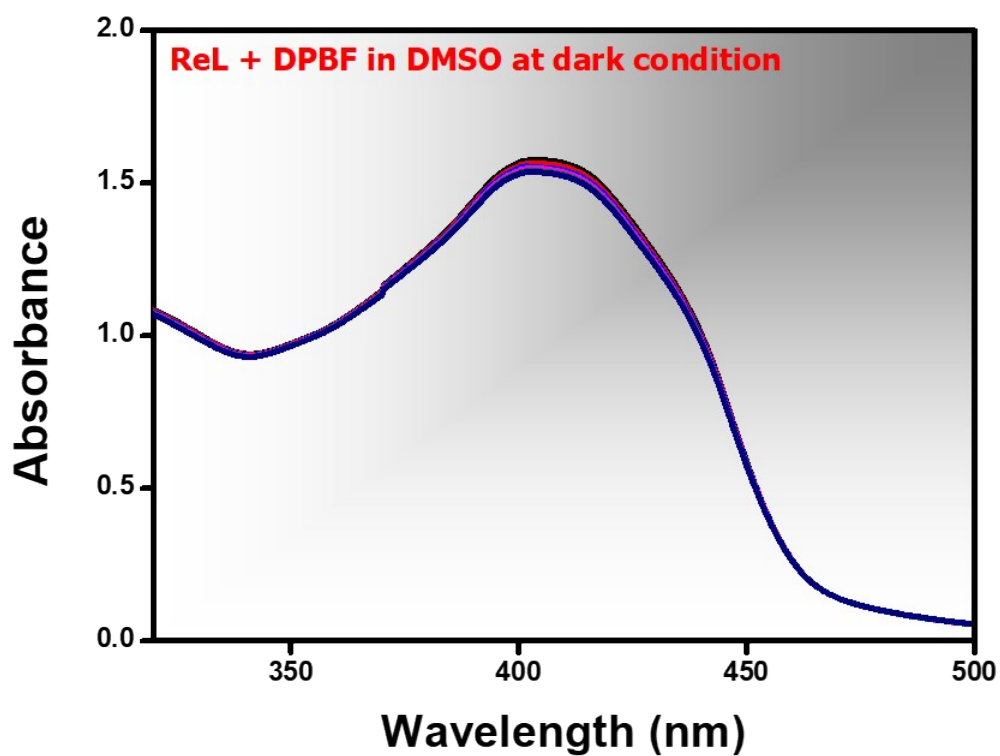
(d)



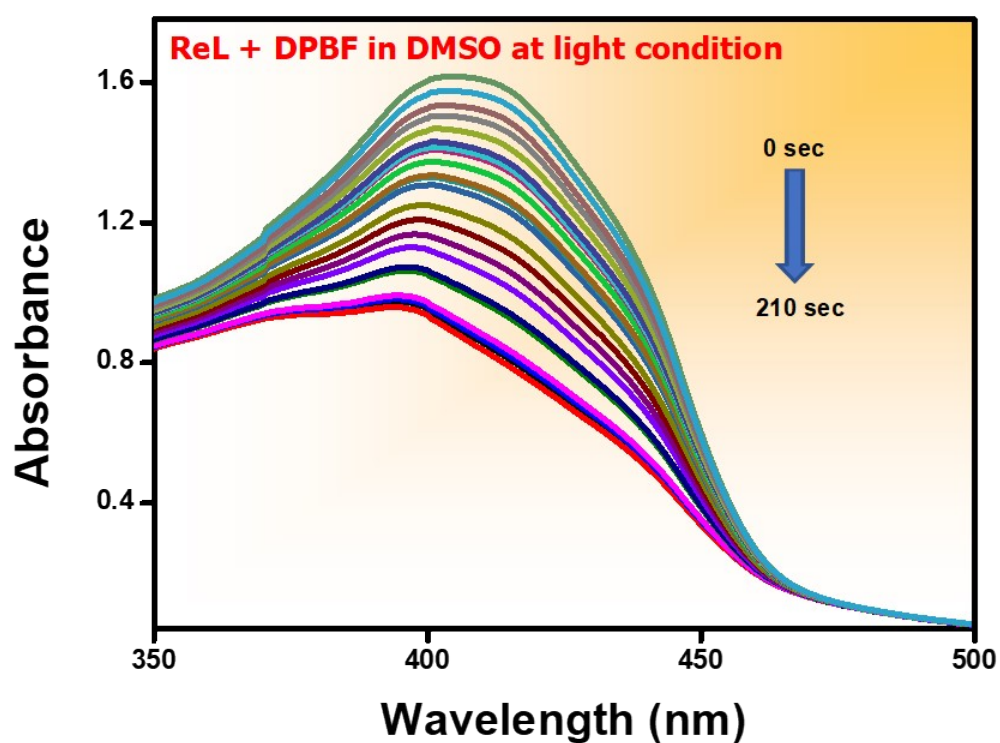
(e)



(f)



(g)



(h)

**Fig. S16: Change in absorbance of DPBF with RB (Rose Bengal), RuL, IrL & ReL in the absence of light (a,c,e,g) and presence of light (b,d,f,h)**

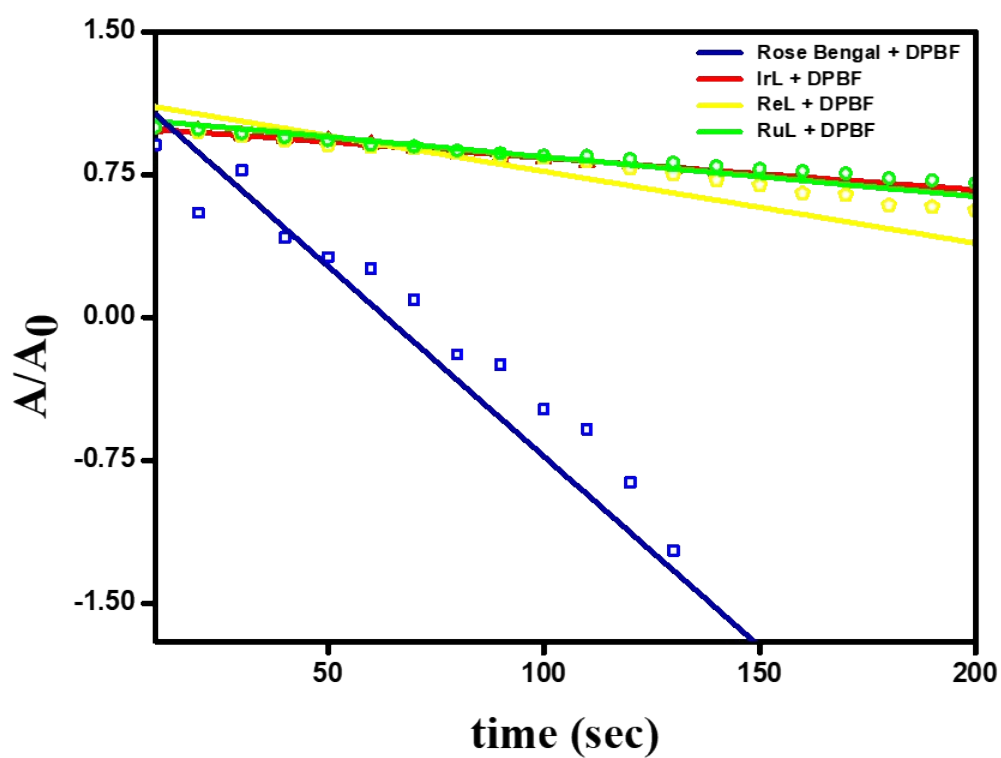
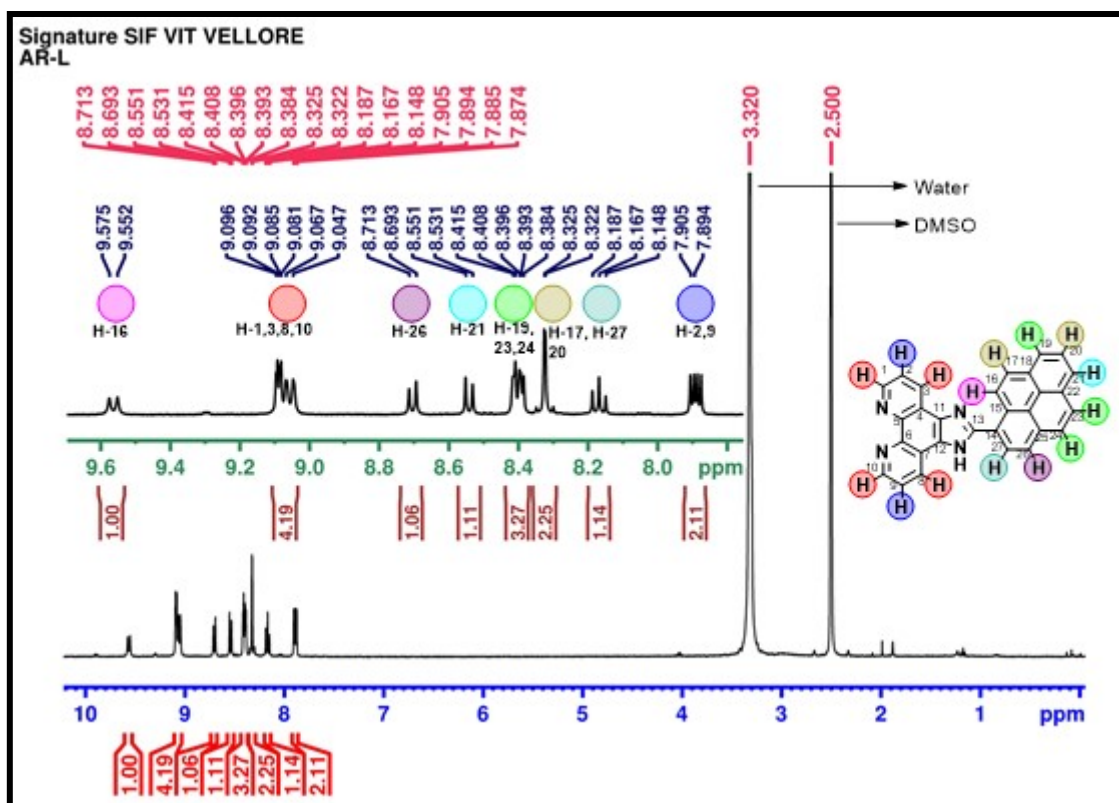
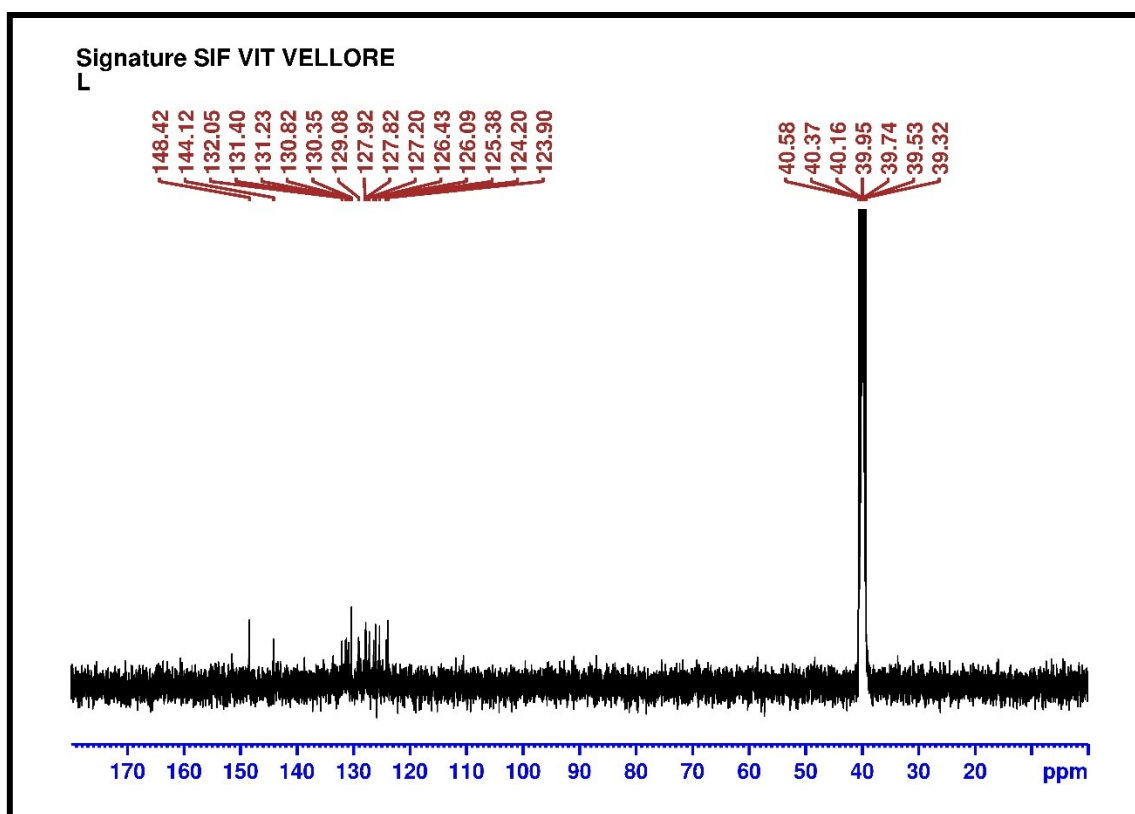


**Fig. S17: Plot of the relative change of absorbance ( $A/A_0$ ) vs. time (sec) of RB (Rose Bengal), RuL, IrL, & ReL**

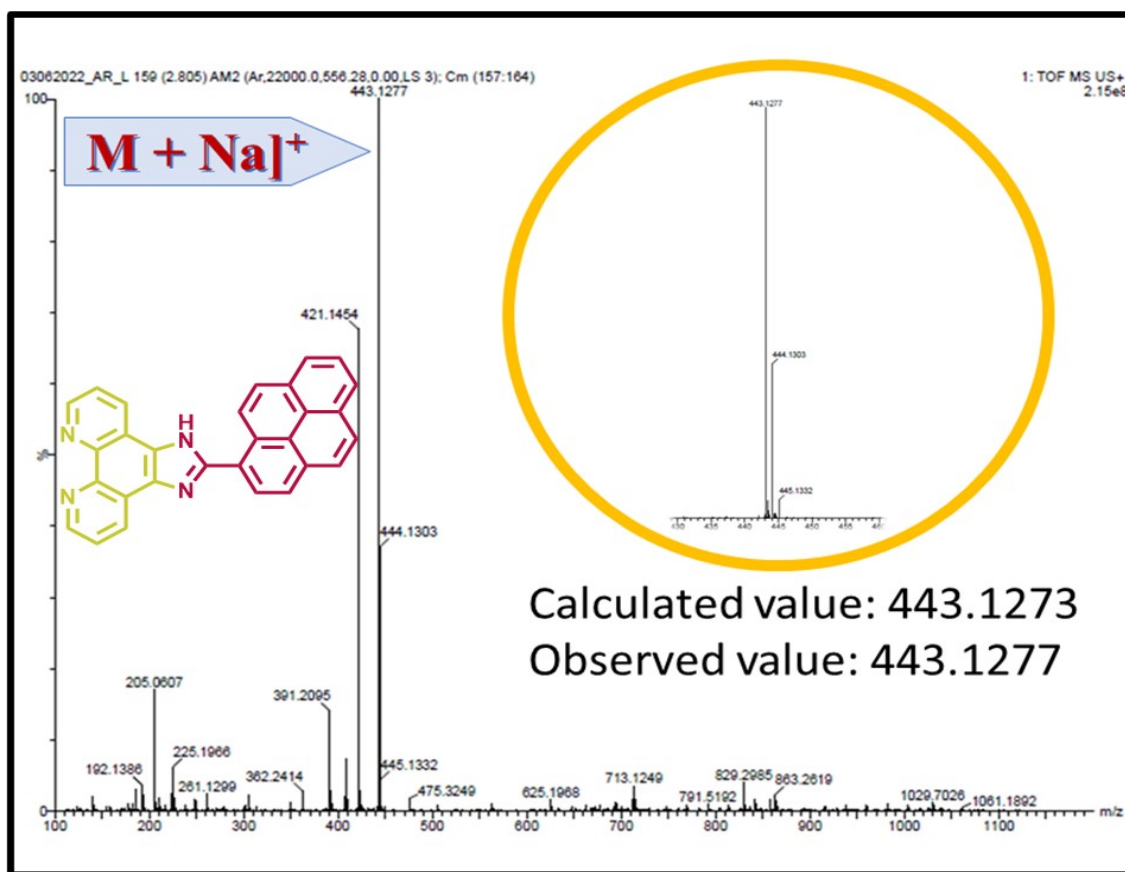
# <sup>1</sup>H NMR of L:



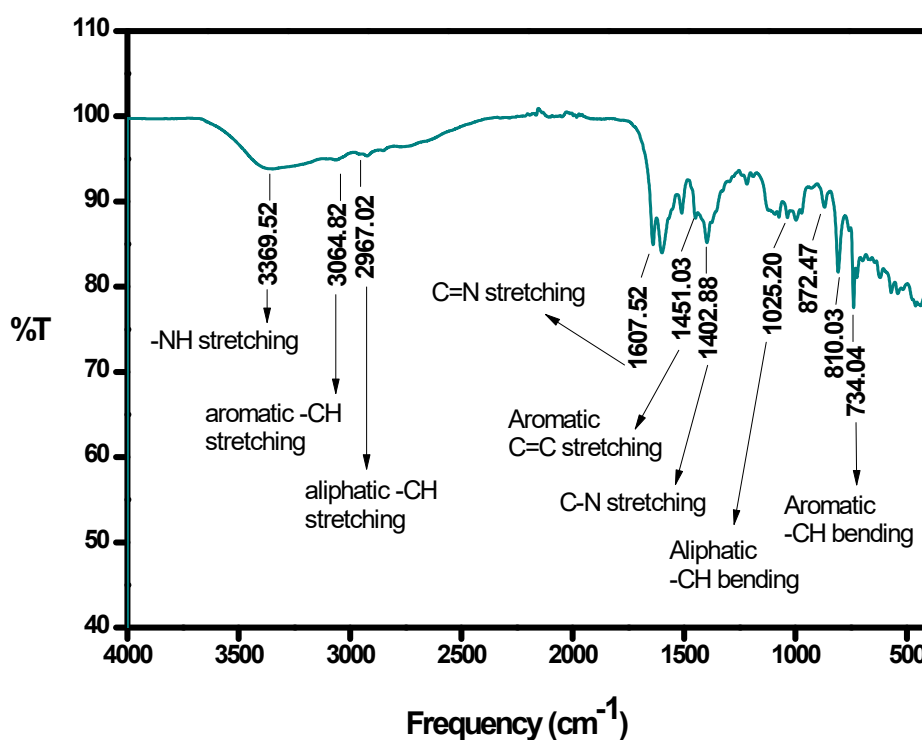
# <sup>13</sup>C NMR of L:



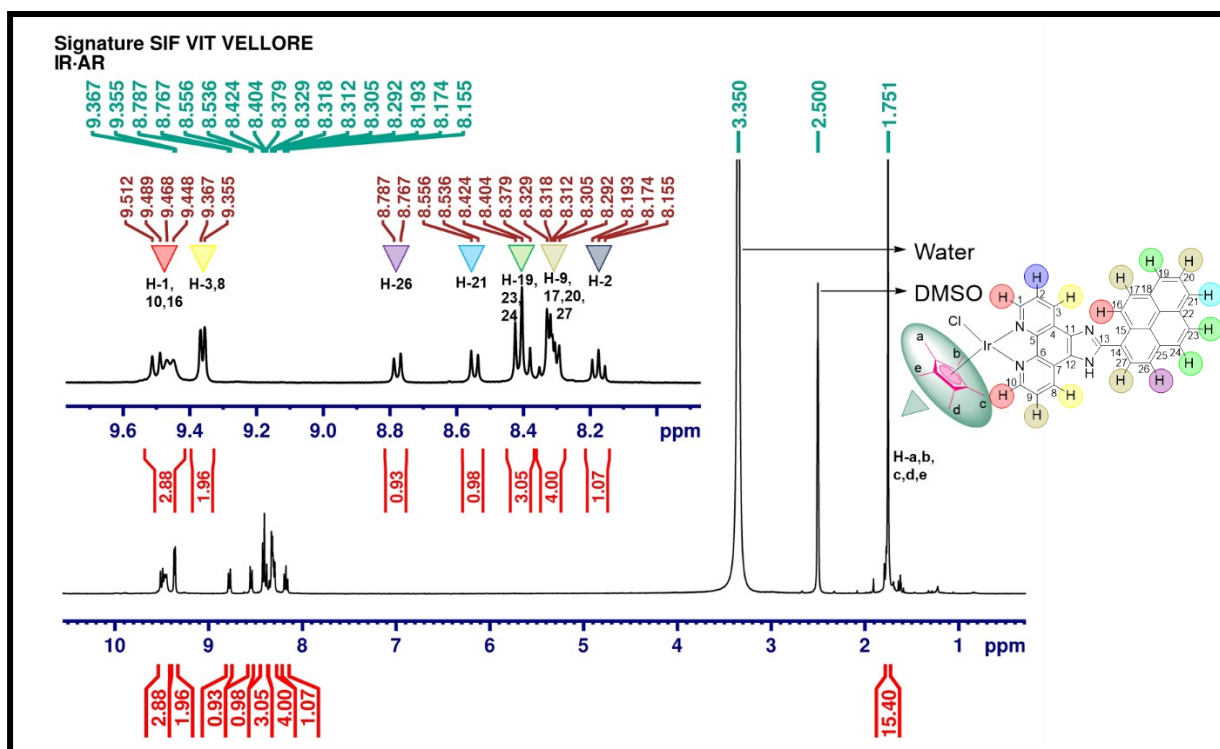
## HRMS of L:



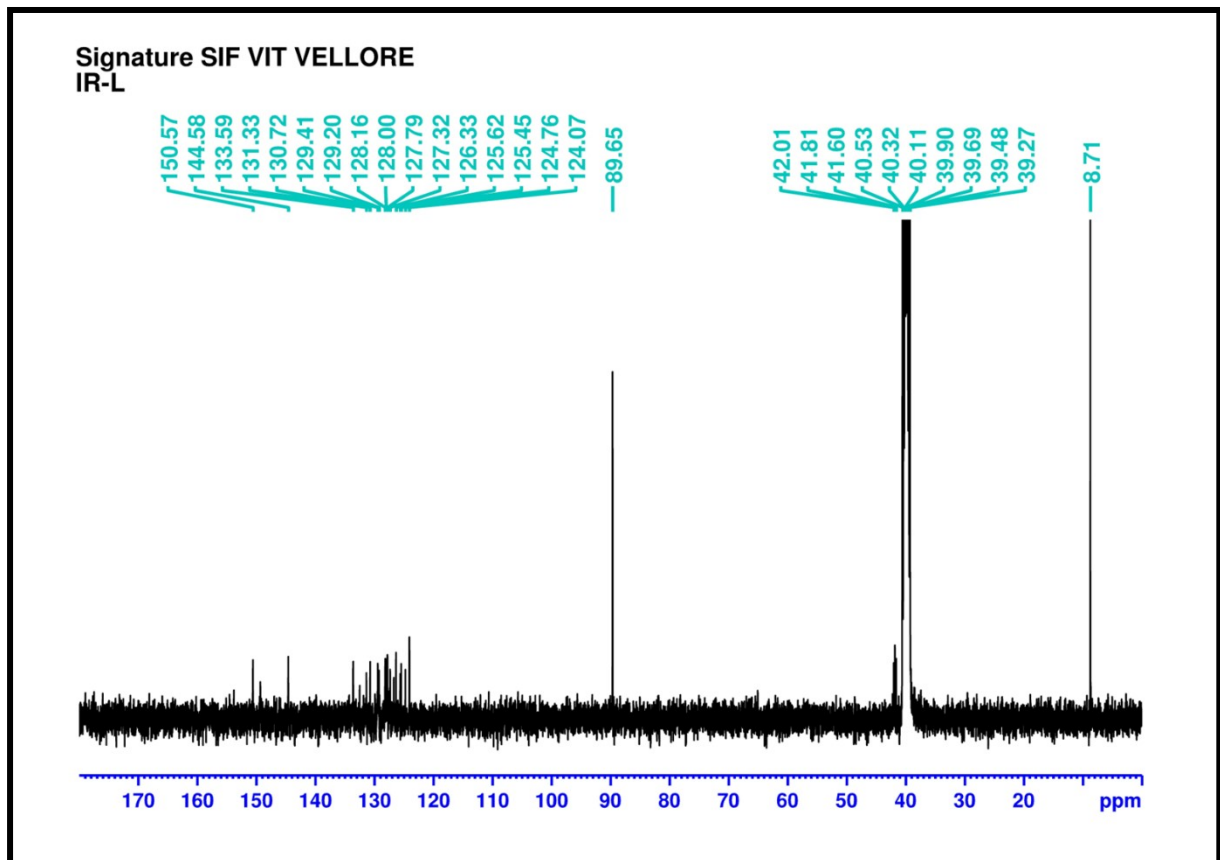
## IR spectra of L:



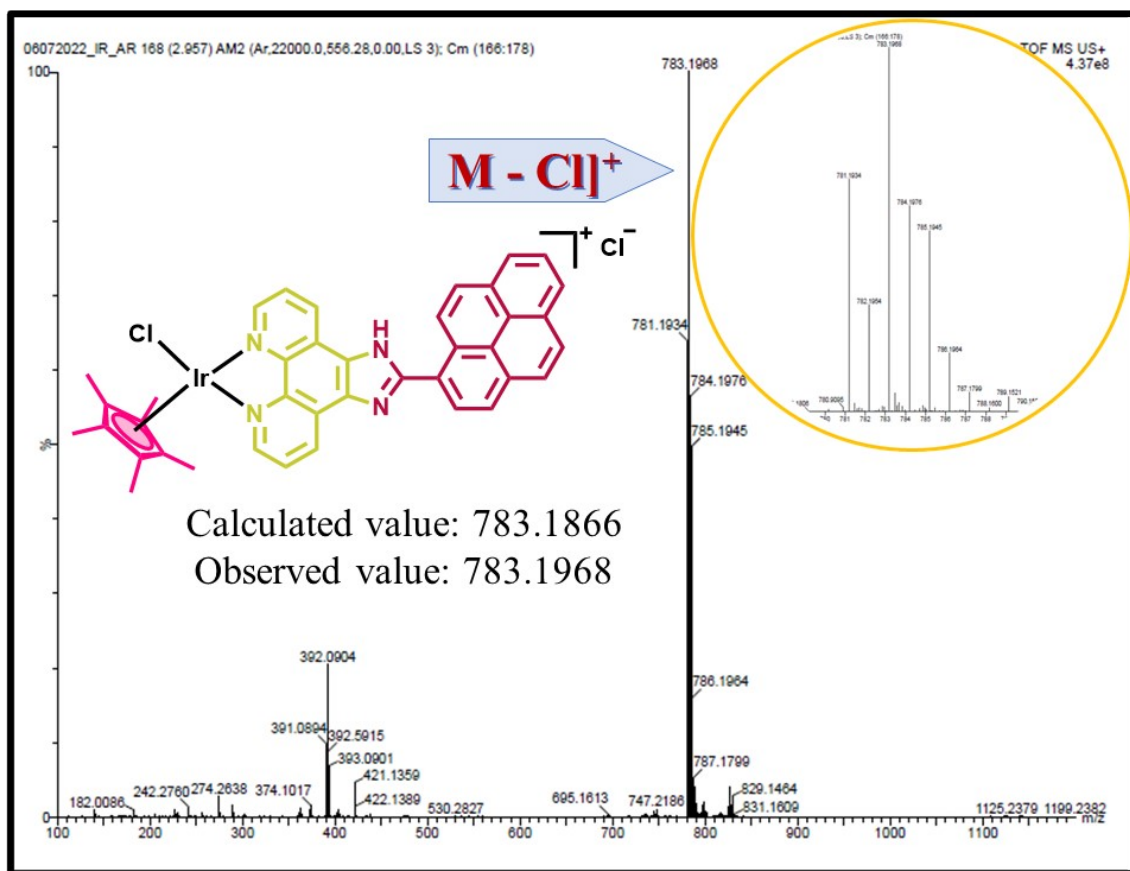
# <sup>1</sup>H NMR of IrL:



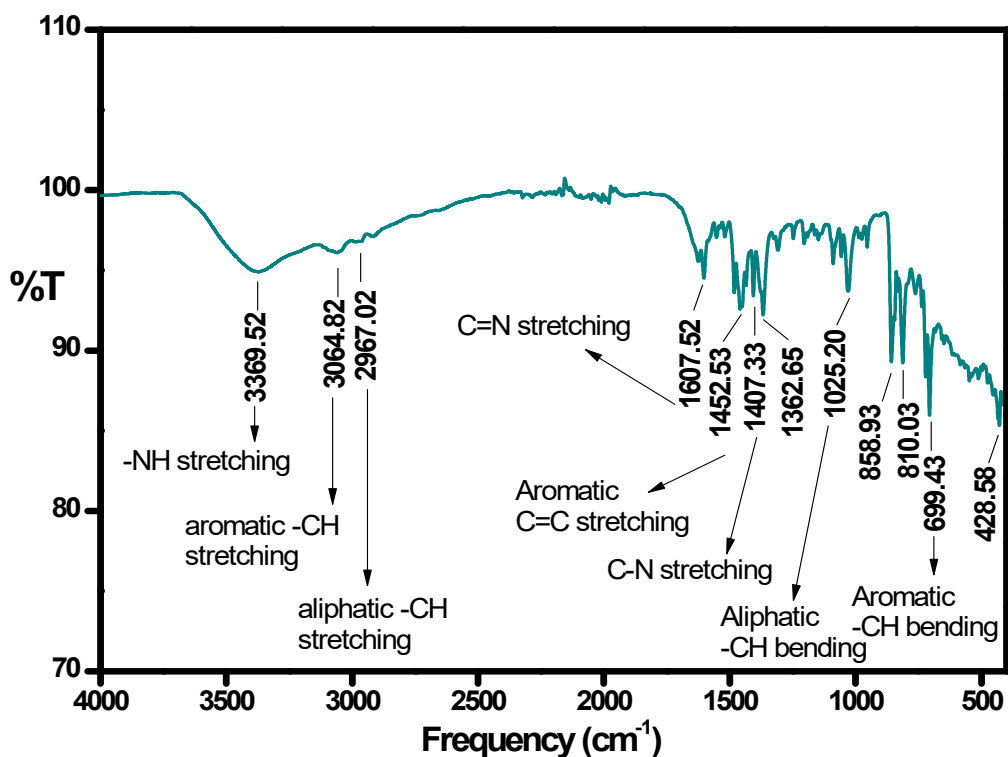
# <sup>13</sup>C NMR of IrL:



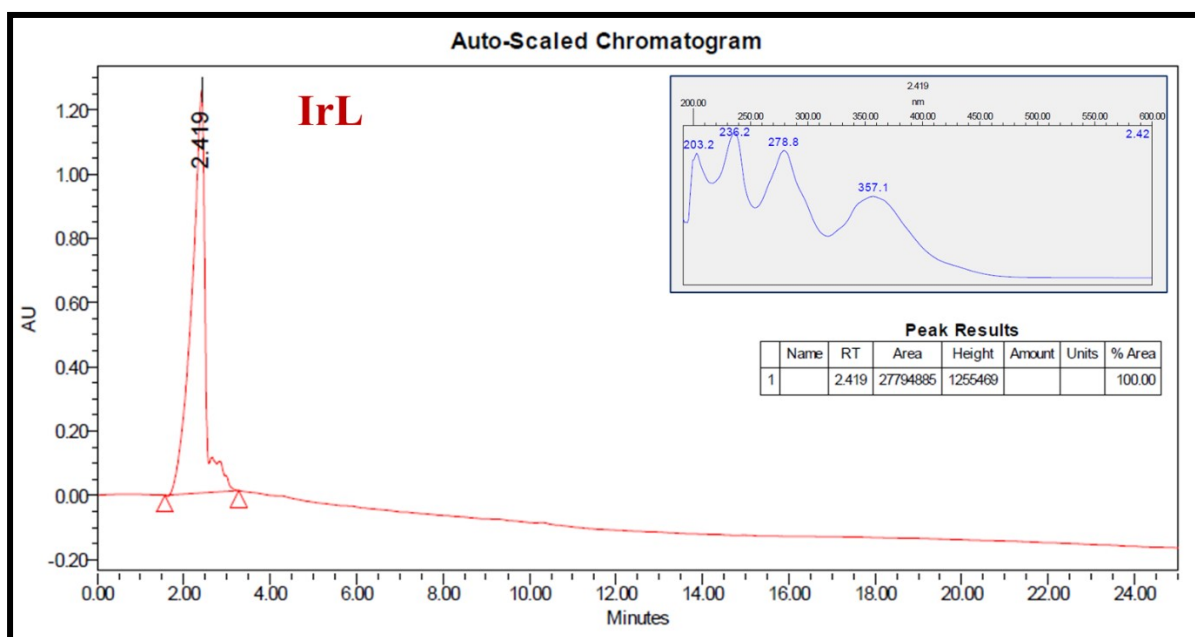
## HRMS of IrL:



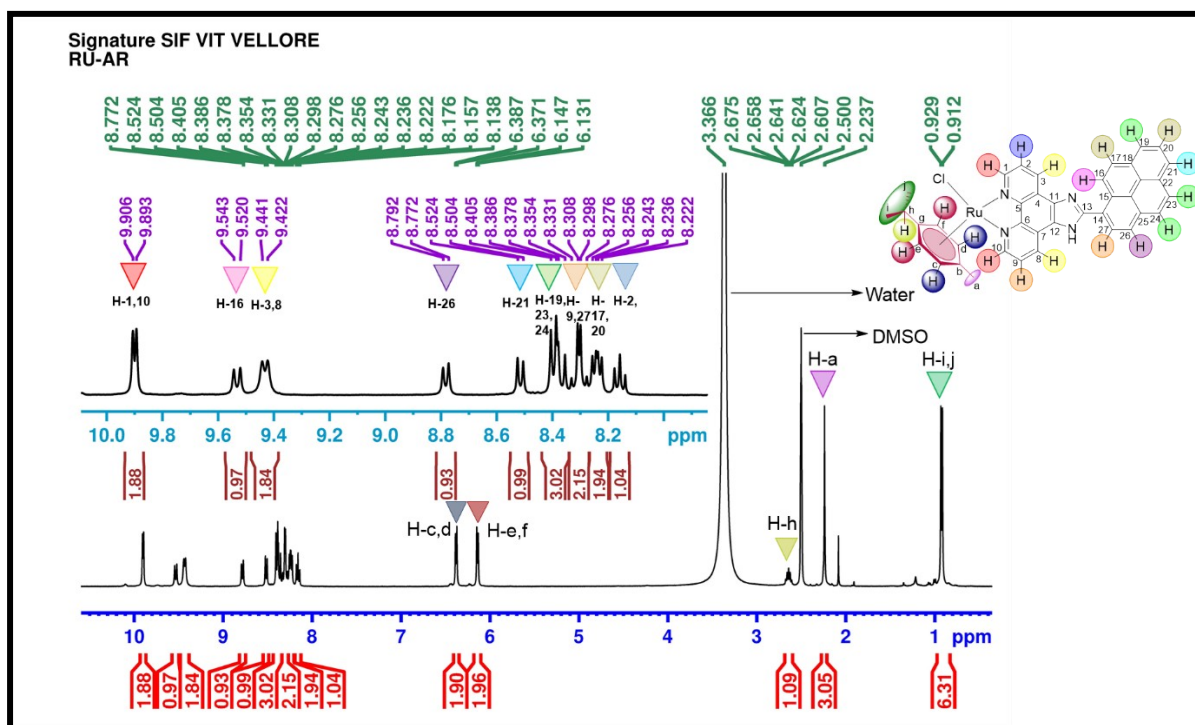
## IR spectra of IrL:



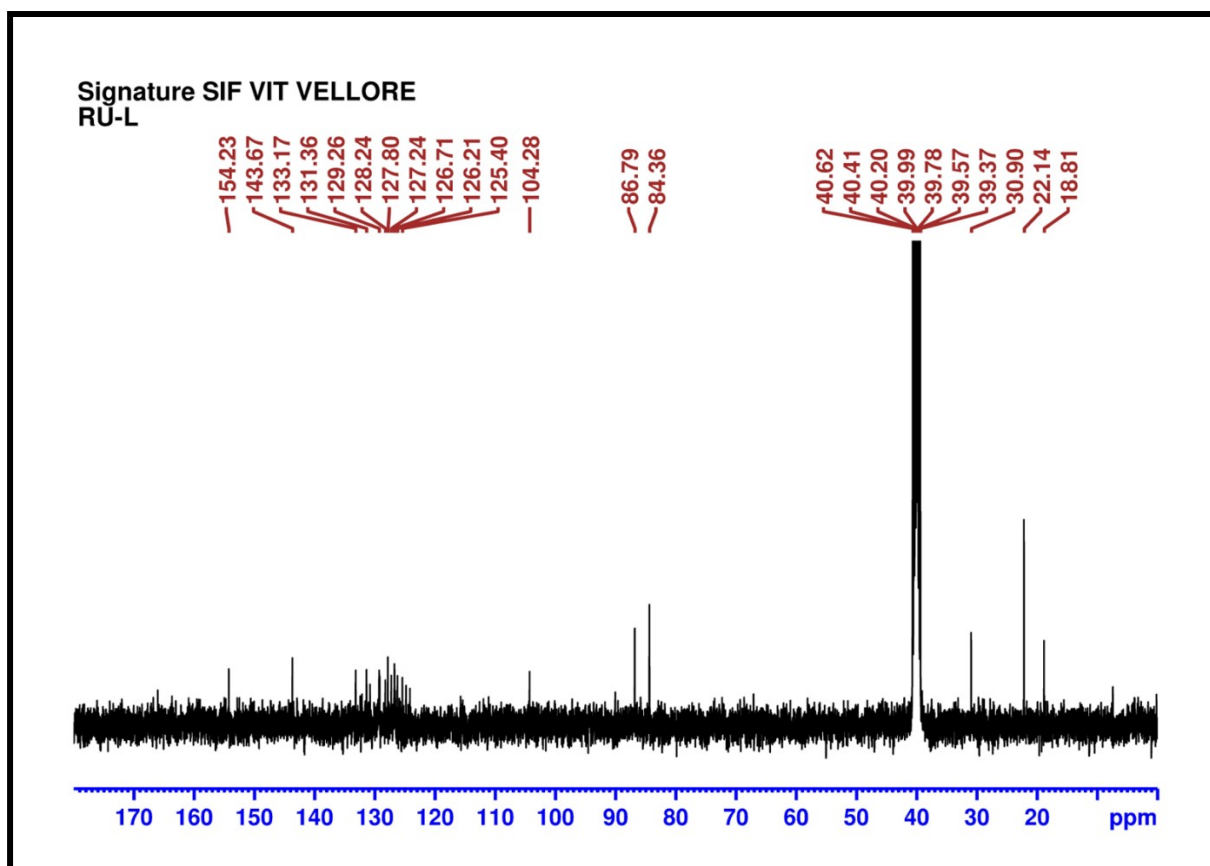
## UPLC data:



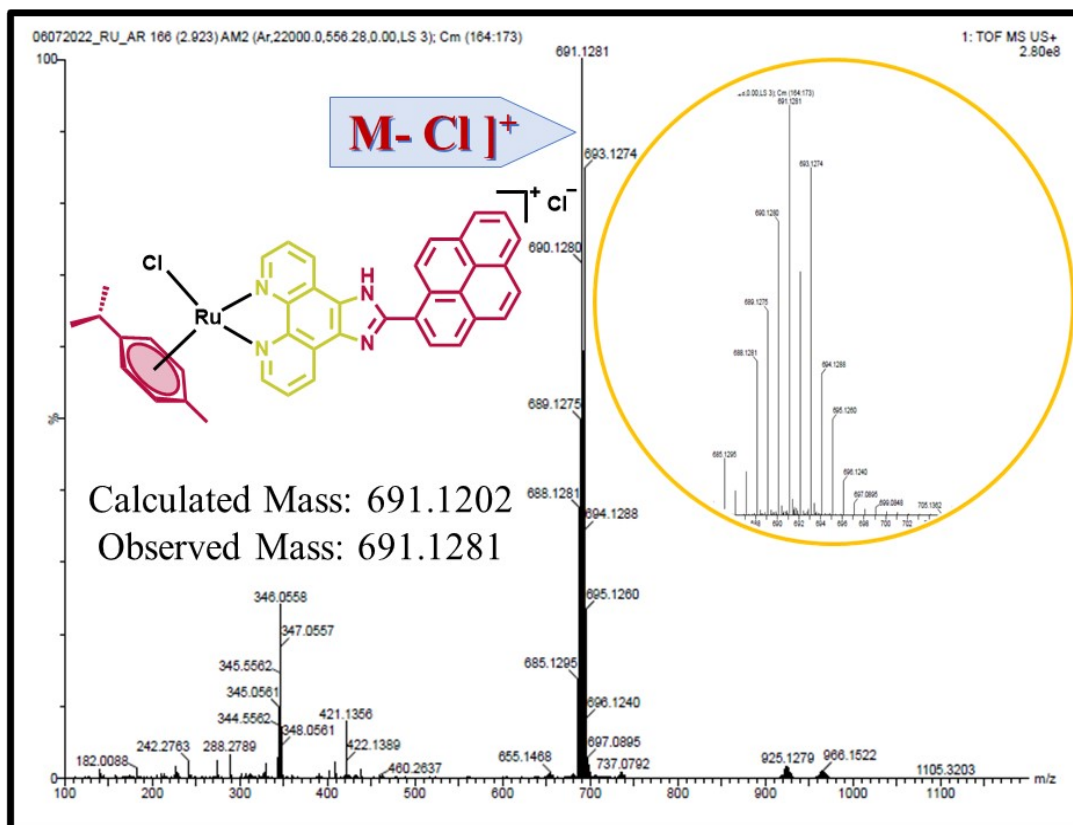
## $^1\text{H}$ NMR of RuL:



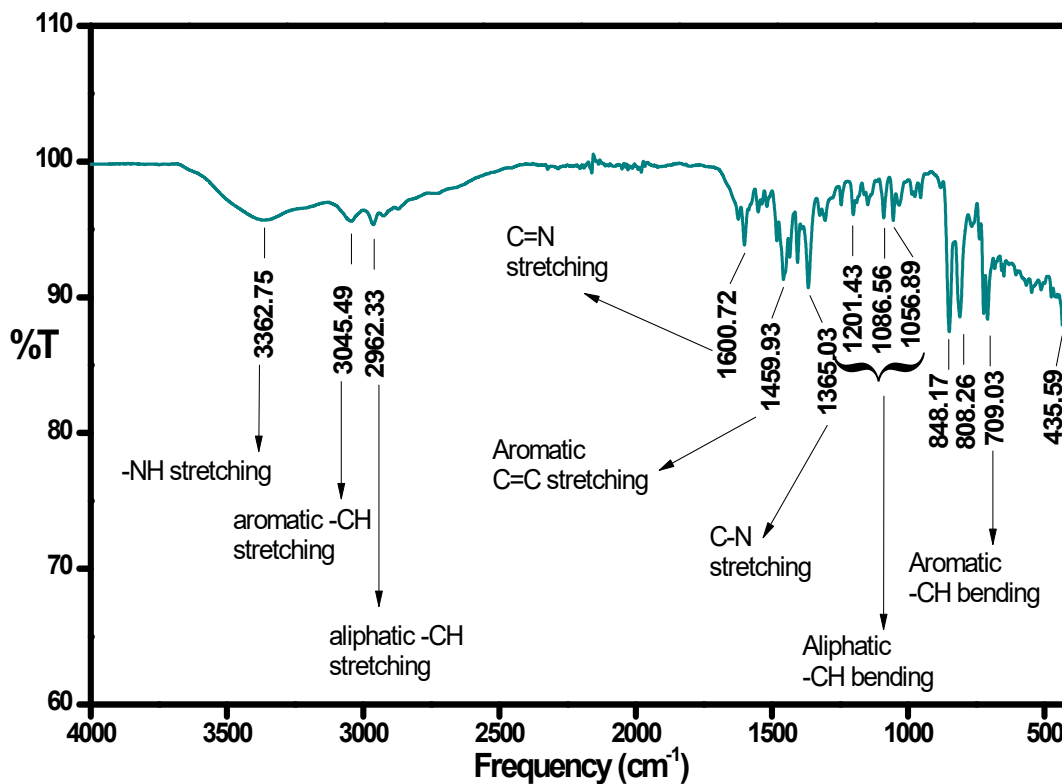
## <sup>13</sup>C NMR of RuL:



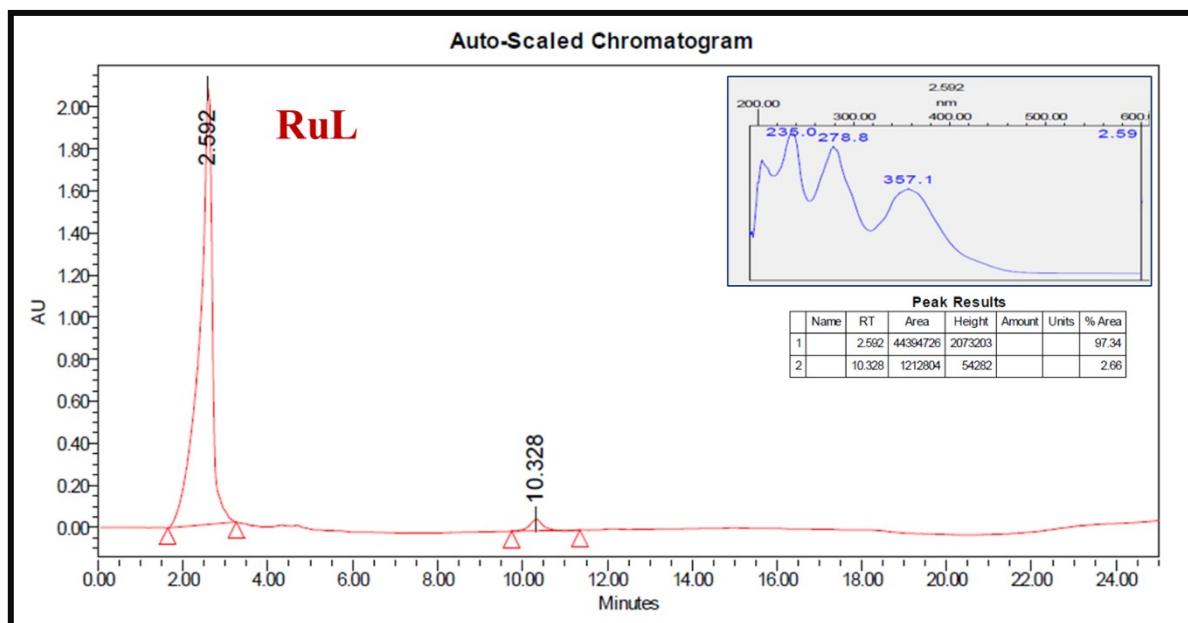
## HRMS of RuL:



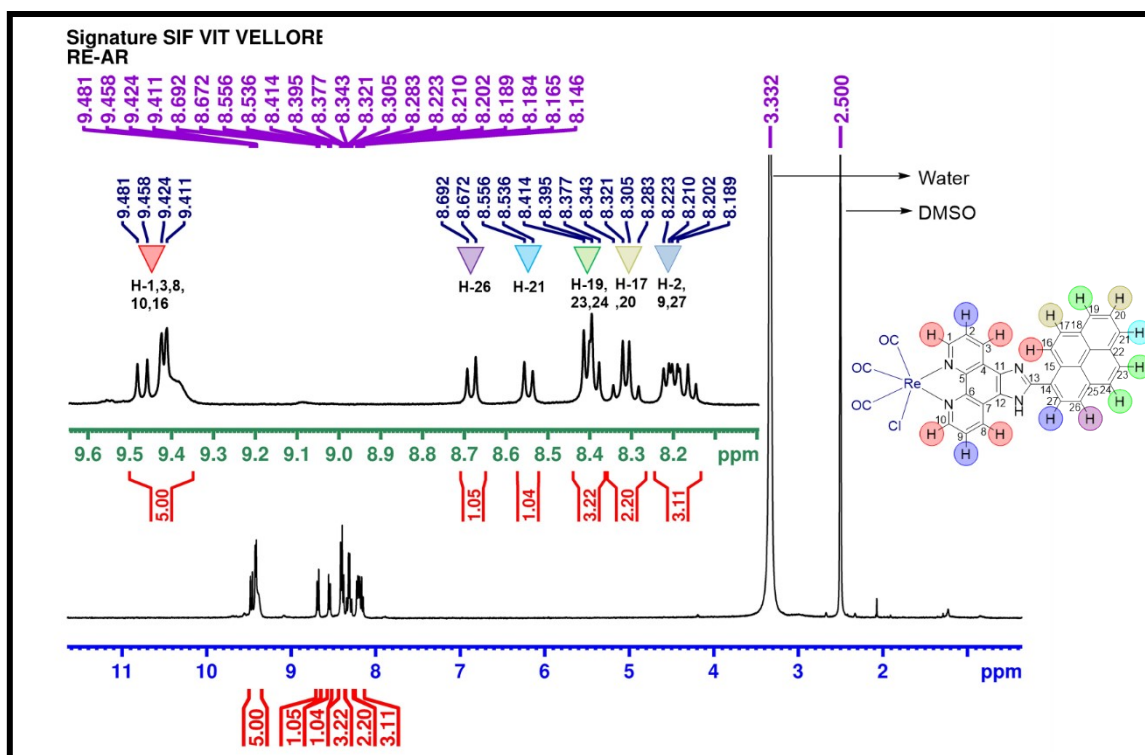
## IR spectra of RuL:



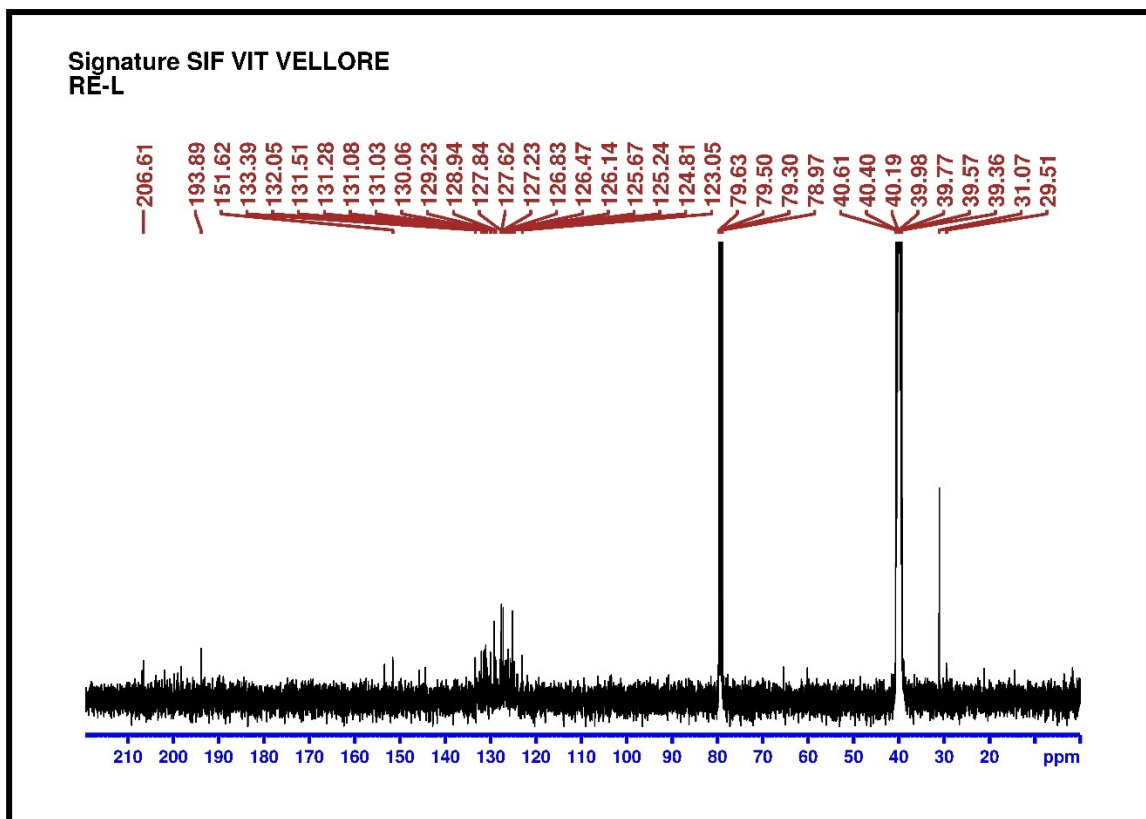
## UPLC data:



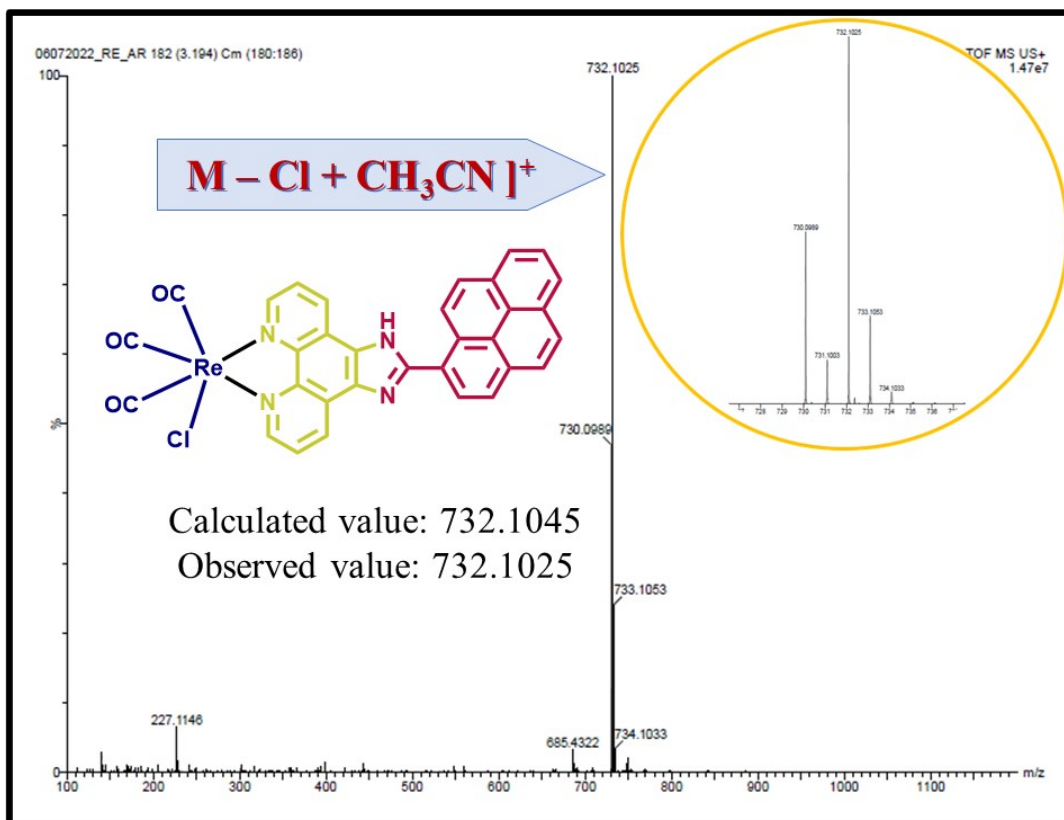
# <sup>1</sup>H NMR of ReL:



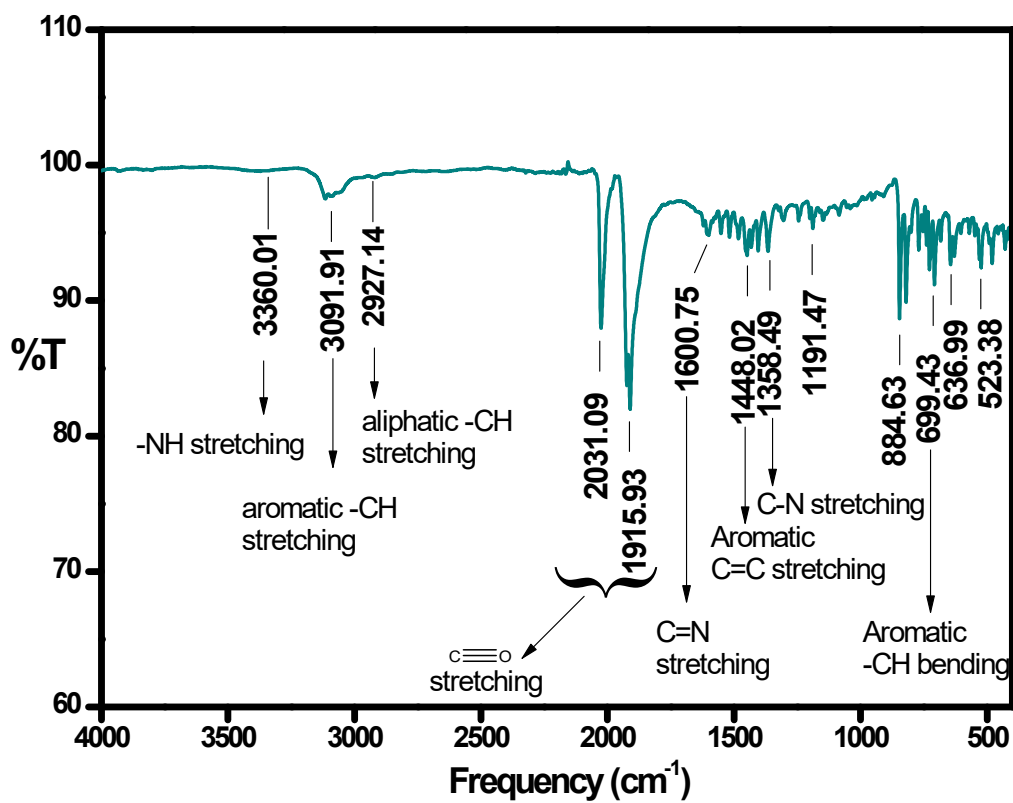
# <sup>13</sup>C NMR of ReL:



# RMS of ReL:



### IR spectra of ReL:



## UPLC data:

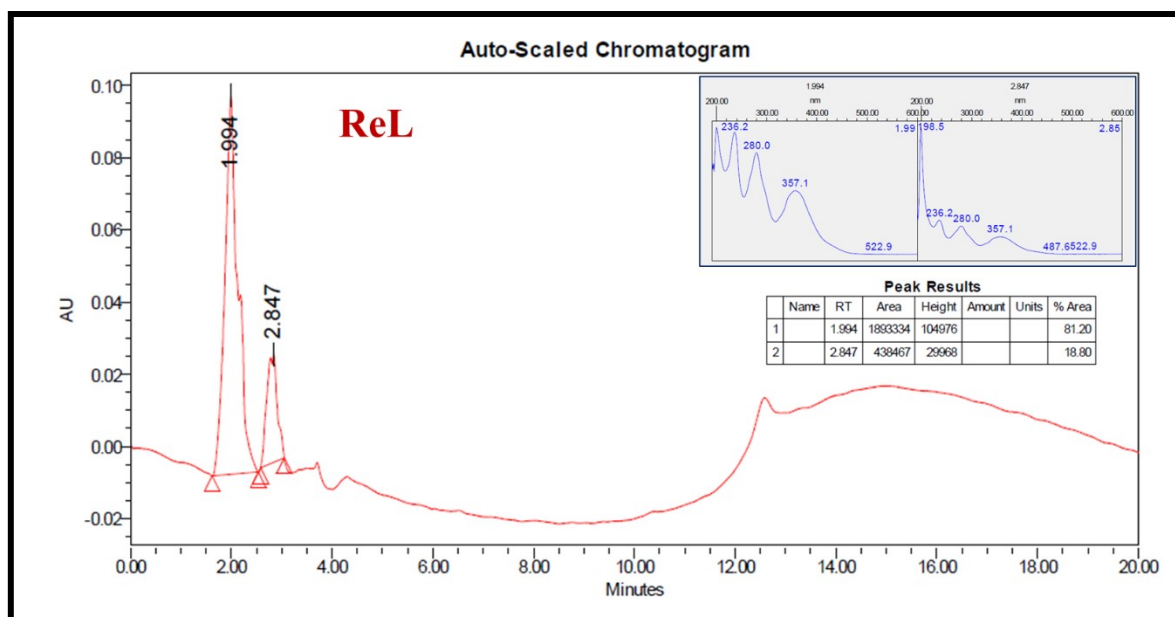


**Table S1. Light and dark toxicity of all the synthesized complexes against HEK-293**

Complex	IC <sub>50</sub> (μM) <sup>a</sup>					
	HEK-293 <sup>b</sup>					
	(in absence of GSH)			(in presence of GSH)		
	Dark	In light	PI <sup>d</sup>	Dark	In light	PI
[RuL]	100.12±0.89	97.41±0.59	1.03	104.42±0.91	96.41±0.38	1.08
[IrL]	102.22±0.77	95.70±0.47	1.07	108.12±0.78	95.70±0.49	1.13
[ReL]	98.14±0.19	96.12±1.19	1.02	103.12±0.38	98.12±1.10	1.05
Cisplatin	45.56±0.62	44.23±0.88	1.03	65.56±0.67	60.23±0.46	1.08

<sup>a</sup>IC<sub>50</sub>: 50% of cells experiences cell death. <sup>b</sup>triple negative human breast cell line. <sup>c</sup>immortalized human embryonic kidney cells lines. <sup>d</sup>PI: Phototoxicity index

## Experimental Procedure:

### UV–visible studies

Three compounds were studied using UV and fluorescence in a 10% DMSO solution. Then, using a 10% DMSO solution and a well-characterized reference with a known quantum yield value, the luminescence quantum yields ( $\phi$ ) were determined using the comparative William's

technique.<sup>1</sup> Quinine Sulphate was used as a benchmark. Quantum yield was calculated with the help of the equation is

$$\varphi_S = \varphi_R \times \frac{I_S}{I_R} \times \frac{OD_R}{OD_S} \times \frac{\eta_S}{\eta_R} \dots\dots\dots (i)$$

Where,  $\varphi$  = quantum yield, OD = absorbance at  $\lambda_{max}$ , I = peak area (area under the curve),  $\eta$  = refractive index of solvent(S), reference (R)

### DNA binding study

The binding of the complexes with calf-thymus DNA (CT-DNA) were observed by electronic spectra and competitive binding assay using ethidium bromide (EtBr) as quencher by fluorescence spectroscopy.

### UV-visible studies

DNA binding assay study was carried out in Tris-HCl buffer (5 mM Tris-HCl in water, pH 7.4) in aqueous medium for the complexes. The concentration of CT-DNA was calculated from the absorbance intensity at 260 nm and molar absorption coefficient value ( $6600 \text{ M}^{-1} \text{ cm}^{-1}$ ). Same amount of DNA was added in the sample and reference in cuvettes. Then titration was carried out with increasing the concentration of CT-DNA from 0 to 50  $\mu\text{M}$ . Sample was equilibrated with CT-DNA for about 5 min and then absorbance of the complex was measured.<sup>2</sup> The  $K_b$  value (intrinsic DNA binding constant) was calculated with the help of equation (ii)

$$\frac{DNA}{(\varepsilon_a - \varepsilon_f)} = \frac{DNA}{(\varepsilon_b - \varepsilon_f)} + \frac{1}{k_b(\varepsilon_a - \varepsilon_f)} \dots\dots\dots(ii)$$

Where, [DNA] = concentration of DNA in the base pairs,  $\varepsilon_a$  = apparent extinction coefficient observed for the complex,  $\varepsilon_f$  = extinction coefficient of the complex in its free form,  $\varepsilon_b$  = extinction coefficient of the complex when fully bound to DNA. From the resulting data we got [DNA]/( $\varepsilon_a - \varepsilon_f$ ) vs. [DNA] linear plot with the help of Origin Lab, version 8.5. From the ratio of slope and intercept we got the intrinsic binding constants ( $K_b$ ).

### Ethidium bromide displacement assay

The ethidium bromide (EtBr) displacement assay was carried out to explain the mode of binding between the potent compounds with DNA.<sup>3</sup> The apparent binding constant ( $K_{app}$ ) of the complexes [RuL], [IrL] and [ReL] to CT-DNA were calculated using ethidium bromide (EtBr) as a spectral probe in 5 mM Tris-HCl buffer (pH 7.4). EtBr does not exhibit any fluorescence in its free form as its fluorescence is quenched by the solvent molecules. But its fluorescence intensity increases in presence of CT-DNA, which suggests the intercalative mode of binding of EtBr with DNA grooves. The fluorescence intensity was found to decrease with a further increase in the concentration of the complexes. Thus, it can be said that the complexes displace EtBr from CT-DNA grooves and the complexes themselves get

bound to the DNA base pairs. The values of the apparent binding constant ( $K_{app}$ ) were calculated from the following equation:

$$K_{app} \times [Complex]_{50} = k_{EtBr} \times [EtBr] \dots\dots\dots(iii)$$

Where  $K_{EtBr}$  is the EtBr binding constant ( $K_{EtBr} = 1.0 \times 10^7 \text{ M}^{-1}$ ), and  $[EtBr] = 8 \times 10^{-6} \text{ M}$ . Stern-Volmer equation has been employed for the quantitative determination of the Stern-Volmer quenching constant ( $K_{SV}$ ).<sup>4</sup> Origin 8.5 software was used to plot the fluorescence data to obtain the linear plot of  $I_0/I$  vs. [complex]. The value of  $K_{SV}$  were obtained by using the equation

$$\frac{I_0}{I} = 1 + K_{SV}[Q] \dots\dots\dots (iv)$$

**n-Octanol-water partition coefficient (log  $P_{o/w}$ ):**

The log  $P_{o/w}$  of these complexes was calculated via shake flask method using the previously published procedure.<sup>9</sup> A known amount of each complex was suspended in water (presaturated with n-octanol) and shaken for 48 h on an orbital shaker.<sup>5</sup> To allow the phase separation, the solution was centrifuged for 10 min at 3000 rpm. After the separation of two layers, they were subjected to UV-Vis spectroscopic analysis. The partition coefficient (log  $P_{o/w}$ ) values were calculated using the OD of the complex in water and octanol.

**Protein (BSA) binding studies**

Serum albumin proteins are major component in blood plasma proteins and plays significant roles in drug transport and metabolism.<sup>6</sup> The interaction of the drug with bovine serum albumin (BSA), a structural homologue with human serum albumin (HSA) has been studied from tryptophan emission quenching experiment. Tryptophan emission quenching experiment was performed to detect the interaction of the complexes with protein BSA. Initially, BSA solution ( $2 \times 10^{-6} \text{ M}$ ) was prepared in Tris- HCl/NaCl buffer. The aqueous solutions of the complexes were subsequently added to BSA solution with increase their concentrations. After each addition, the solutions were shaken slowly for 5 min before recording the fluorescence at a wavelength of 295 nm ( $\lambda_{ex} = 295 \text{ nm}$ ). A gradual decrease in fluorescence intensity of BSA at  $\lambda = 340 \text{ nm}$  was observed upon increasing the concentration of complex, which confirms that the interaction between the complex and BSA is occurred. Stern-Volmer equation has been employed to quantitatively determine the quenching constant ( $K_{BSA}$ ).<sup>6</sup> Origin Lab 8.5 was used to plot the emission spectral data to obtain linear plot of  $I_0/I$  vs. [complex] using following equation (v):

$$\frac{I_0}{I} = 1 + K_{BSA}[Q] = 1 + K_q\tau_0[Q] \dots\dots\dots(v)$$

Where  $I_0$  is the fluorescence intensity of BSA in absence of complex and  $I$  indicate the fluorescence intensities of BSA in presence of complex of concentration  $[Q]$ ,  $\tau_0$  = lifetime of the tryptophan in BSA found as  $1 \times 10^{-8}$  and  $k_q$  is the quenching constant. Scatchard equation

(vi) gives the binding properties of the complexes.<sup>7</sup> Where K = binding constant and n = number of binding sites.

$$\log \frac{I_0 - I}{I} = \log K + n \log [Q] \dots\dots(vi)$$

**Stability study**

The stability of the metal complexes was checked in 10% DMSO in water, 1mM cysteine (aqueous) and aqueous GSH (1mM) medium.

**Conductivity measurement:**

The conductivity of the complexes were determined with the help of conductivity-TDS meter-307 (Systronics, India) and cell constant 1.0 cm<sup>-1</sup> due to the confirming the interaction of the complexes with DMSO, aqueous DMSO, GSH, and Ct-DNA solutions.<sup>8</sup> For this experiment we used the complex concentration 3×10<sup>-5</sup> M.

**Viscosity measurement**

In order to find out the binding mode of drugs, using complexes has treated DNA; a hydrodynamic method like viscosity study has been conducted using Ostwald Viscometer. The result was also compared with EtBr.

**The quantum yield of singlet oxygen determination:<sup>9</sup>**

The singlet oxygen (<sup>1</sup>O<sub>2</sub>) quantum yields of the complex RuL4 at ambient temperature in DMSO were calculated using visible light (400–700 nm) for photosensitization. The <sup>1</sup>O<sub>2</sub> quantum yields were determined by monitoring the photooxidation of DPBF after sensitization by the complex. DPBF is a convenient acceptor because it absorbs in the region where the dye is transparent and rapidly scavenges singlet oxygen to generate colorless products. This reaction occurs with little or no physical quenching. The solutions contained dyes in low concentrations and had optical densities ranging from 0.12 to 0.16 to minimize the possibility of <sup>1</sup>O<sub>2</sub> quenching by the dyes. The photooxidation of DPBF was monitored from 20 s to 200 s. The quantum yield of <sup>1</sup>O<sub>2</sub> was calculated relative to optically matched solutions and compared the quantum yield of DPBF photooxidation after sensitization by the compound of interest to that of Rose Bengal.

$$\phi\Delta_S = \phi\Delta_{RB} \times \frac{m_S}{m_{RB}} \times \frac{F_{RB}}{F_S} \dots\dots\dots(vii)$$

where S denotes a sample, and RB denotes Rose Bengal. φΔ is the <sup>1</sup>O<sub>2</sub> quantum yield, and m is the slope of the plot of DPBF absorbance at 417 nm vs. irradiation time. O.D is the optical density at the irradiation wavelength and F is the absorption correction factor, which is given by the Equation (viii)

$$F=1-10^{-OD} \dots\dots\dots(viii)$$

## References:

- (1) Shamsi-Sani, M.; Shirini, F.; Abedini, M.; Seddighi, M. Synthesis of Benzimidazole and Quinoxaline Derivatives Using Reusable Sulfonated Rice Husk Ash (RHA-SO<sub>3</sub>H) as a Green and Efficient Solid Acid Catalyst. *Research on Chemical Intermediates* **2016**, *42* (2), 1091–1099. <https://doi.org/10.1007/s11164-015-2075-5>.
- (2) Sirajuddin, M.; Ali, S.; Badshah, A. Drug–DNA Interactions and Their Study by UV–Visible, Fluorescence Spectroscopies and Cyclic Voltametry. *J Photochem Photobiol B* **2013**, *124*, 1–19. <https://doi.org/10.1016/j.jphotobiol.2013.03.013>.
- (3) Dasari, S.; Patra, A. K. Luminescent Europium and Terbium Complexes of Dipyridoquinoxaline and Dipyridophenazine Ligands as Photosensitizing Antennae: Structures and Biological Perspectives. *Dalton Transactions* **2015**, *44* (46), 19844–19855. <https://doi.org/10.1039/C5DT02852C>.
- (4) Keizer, J. Additions and Corrections - Nonlinear Fluorescence Quenching and the Origin of Positive Curvature in Stern-Volmer Plots. *J Am Chem Soc* **1985**, *107* (18), 5319–5319. <https://doi.org/10.1021/ja00304a601>.
- (5) Kubanik, M.; Holtkamp, H.; Söhnel, T.; Jamieson, S. M. F.; Hartinger, C. G. Impact of the Halogen Substitution Pattern on the Biological Activity of Organoruthenium 8-Hydroxyquinoline Anticancer Agents. *Organometallics* **2015**, *34* (23), 5658–5668. <https://doi.org/10.1021/acs.organomet.5b00868>.
- (6) Suryawanshi, V. D.; Walekar, L. S.; Gore, A. H.; Anbhule, P. V.; Kolekar, G. B. Spectroscopic Analysis on the Binding Interaction of Biologically Active Pyrimidine Derivative with Bovine Serum Albumin. *J Pharm Anal* **2016**, *6* (1), 56–63. <https://doi.org/10.1016/j.jpha.2015.07.001>.
- (7) Jeyalakshmi, K.; Haribabu, J.; Balachandran, C.; Swaminathan, S.; Bhuvanesh, N. S. P.; Karvembu, R. Coordination Behavior of *N*, *N'*, *N''*-Trisubstituted Guanidine Ligands in Their Ru–Arene Complexes: Synthetic, DNA/Protein Binding, and Cytotoxic Studies. *Organometallics* **2019**, *38* (4), 753–770. <https://doi.org/10.1021/acs.organomet.8b00702>.
- (8) Nikolić, S.; Rangasamy, L.; Gligorijević, N.; Arandelović, S.; Radulović, S.; Gasser, G.; Grgurić-Šipka, S. Synthesis, Characterization and Biological Evaluation of Novel Ru(II)–Arene Complexes Containing Intercalating Ligands. *J Inorg Biochem* **2016**, *160*, 156–165. <https://doi.org/10.1016/j.jinorgbio.2016.01.005>.
- (9) Musib, D.; Pal, M.; Raza, M. K.; Roy, M. Photo-Physical, Theoretical and Photo-Cytotoxic Evaluation of a New Class of Lanthanide(III)–Curcumin/Diketone Complexes for PDT Application. *Dalton Transactions* **2020**, *49* (31), 10786–10798. <https://doi.org/10.1039/D0DT02082F>.